Reprinted From
Physics of High Energy Density
© 1971, XLVIII Corso
Academic Press Inc. - New York

48, 7-50 (1971)

Shock Waves in Condensed Media (*).

G. E. DUVALL

Shock Dynamics Laboratory, Department of Physics
Washington State University, Pullman, Wash.

In this entire discussion we focus attention on a simple thought experiment. We consider a half-space with free surface normal to the x-axis and located at $x = 0$. The medium of interest lies in the region $x > 0$ or $x < 0$. A uniform pressure is applied to the surface or the surface is given an arbitrary velocity at an arbitrary time, and we inquire about the state of the medium at later times. This apparently restrictive model is in reasonable accord with the geometry and physics of most significant experiments and leads to a great variety of interesting problems.

1. – Basic shock relations.

The continuum differential equations of flow, independent of material properties, are, for one-dimensional plane flow:

$$\partial\varrho/\partial t + \partial\varrho u/\partial x = 0\,, \tag{1}$$

$$\varrho\,\mathrm{d}u/\mathrm{d}t \equiv \varrho\,\partial u/\partial t + \varrho u\,\partial u/\partial x = -\partial p/\partial x\,, \tag{2}$$

$$\mathrm{d}E/\mathrm{d}t = -p\,\mathrm{d}V/\mathrm{d}t; \qquad V = 1/\varrho\,, \tag{3}$$

where t is time, x is Eulerian space co-ordinate, ϱ is density, u is particle or mass velocity, E is internal energy, and p is compressive stress in the x-direction, including all dynamic forces due to viscosity, stress relaxation, etc.

Application of a pressure to the surface of a half-space produces a region of change propagating out from the surface. If we suppose that a very long time has elapsed since the driving pressure was first applied at the free surface, and that pressure has been held at a constant value, p_1, then the region of change in the resulting flow may be supposed far removed from the driving surface. If the half-space fills the region $x > 0$, we may shift the origin of

(*) Research sponsored by the United States Office of Scientific Research under Contract No. AFOSR-69-1758.

co-ordinates to a point deep within the material and suppose that the region of change connects a uniform undisturbed state at $x = +\infty$ to a uniform compressed state at $x = -\infty$. To implement this model, we seek solutions of eqs. (1)-(3) of the form

$$\varrho = \varrho(\xi), \quad u = u(\xi), \quad p = p(\xi), \quad E = E(\xi), \quad V = V(\xi),$$

where $\xi = x - Dt$ and D is a constant propagation velocity. Let the values of variables in the undisturbed state be designated by subscript « 0 » and those in the uniform state at $x = -\infty$ by subscript « 1 ». Then eqs. (1)-(3) can be integrated to yield the relations

$$\varrho(D-u) = \varrho_0(D-u_0), \tag{4}$$

$$p - p_0 = \varrho_0(D-u_0)^2(V_0 - V) = \varrho_0(D-u_0)(u-u_0), \tag{5}$$

$$E - E_0 = \tfrac{1}{2}(p+p_0)(V_0 - V). \tag{6}$$

Substitution of the final-state variables into eqs. (4)-(6) yields the *jump conditions*. They are particularly useful in the forms:

$$\varrho_0/\varrho_1 = 1 - (u_1 - u_0)/(D-u_0), \tag{7}$$

$$(D-u_0)^2 = V_0^2[(p_1-p_0)/(V_0-V_1)], \tag{8}$$

$$E_1 - E_0 = \tfrac{1}{2}(p_1+p_0)(V_0-V_1). \tag{9}$$

The undisturbed medium will usually be at rest. In deriving eqs. (4)-(9) it has been assumed to have a velocity u_0. The generality obtained by this assumption will at times be useful.

Any travelling wave which connects end states « 1 » and « 0 » and which satisfies eqs. (7)-(9) is called a *shock wave*. The locus of states (p_1, V_1) which satisfy eqs. (7)-(9) is called the « Rankine-Hugoniot (p, V) curve centered at (p_0, V_0) » or, more simply, the « Hugoniot » or « R-H curve ». It is also sometimes called the « dynamic adiabat » or « shock adiabat ». When the root of eq. (8) is taken, a duality of sign appears. If $D - u_0 > 0$ the compressed state lies to the left, the undisturbed state to the right, and the disturbance is a « forward-facing shock wave ».

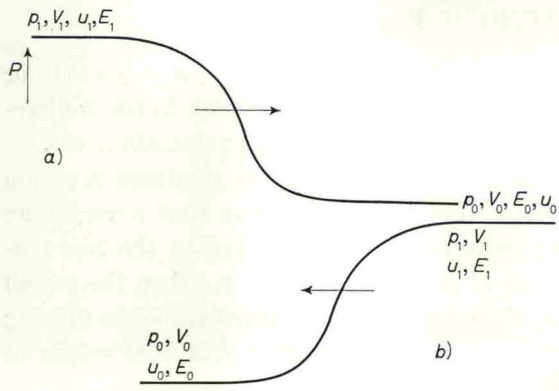

Fig. 1. – *a*) Forward-facing shock wave, $D - u_0 > 0$.
b) Backward-facing shock wave, $D - u_0 < 0$.

If $D-u_0<0$, the undisturbed and compressed regions are interchanged and we have a « backward-facing shock wave ». These two cases are illustrated in Fig. 1.

Material is always accelerated in the direction of propagation of the shock wave. From eqs. (7)-(9) the change in mass flow or particle velocity can be calculated:

$$u_1-u_0=\pm[(p_1-p_0)(V_0-V_1)]^{\frac{1}{2}}. \tag{10}$$

If $D-u_0>0$, $u_1-u_0>0$; if $D-u_0<0$, $u_1-u_0<0$.

Equation (9) contains the thermodynamics of the shock transition and is called the « Rankine-Hugoniot equation ». For « normal » materials it can be satisfied only by compressive waves, $p_1>p_0$. We arbitrarily define « normal » materials as those for which the adiabatic (p, V) relation in one-dimensional compression, sometimes called « uniaxial strain », is concave upward. Most fluids are normal in this sense, and most solids are normal over a restricted range. For such materials the limitation of shock waves to compressive waves follows from both hydrodynamic and thermodynamic considerations. As to the latter, we find that by differentiating eq. (9) and combining it with the First and Second Laws of Thermodynamics an expression is obtained for entropy change along the Hugoniot:

$$\mathrm{d}S_1/\mathrm{d}p=[(V_0-V_1)/2T_1]\left[1-\frac{(p_1-p_0)/(V_0-V_1)}{|\mathrm{d}p/\mathrm{d}V|_{V_1}}\right], \tag{11}$$

where T_1 is temperature at (p_1, V_1). The bracket in eq. (11) is positive for all $p_1>p_0$ if the Hugoniot is concave upward. This is illustrated in Fig. 2, where it is obvious that the slope of the chord from 0 to A is less in magnitude than the slope of the tangent at A.

The increase in entropy in the shock front is produced by the presence of dynamic or irreversible forces associated with viscosity, stress-relaxation and the like. These forces are responsible for maintaining the linear relation between p and V in eq. (5): at any point of compression the total compressive stress p in the x-direction is the sum of an equilibrium and of a dynamic contribution. A physically unreal but mathematically interesting problem is to let the dynamic stress vanish and to represent the equilibrium stress by an equation of state,

$$p=\overline{p}(V, E).$$

In the absence of other irreversible processes, such as heat conduction, the shock front then becomes a mathematical discontinuity connecting states (p_0, V_0, u_0, E_0) and (p_1, V_1, u_1, E_1) [1].

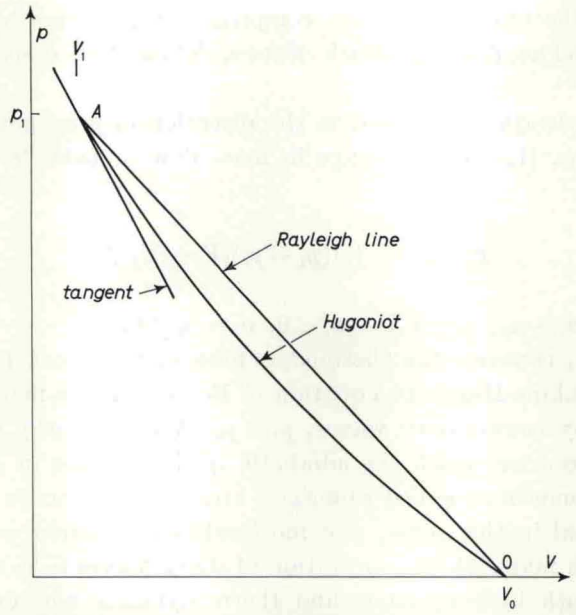

Fig. 2. – Entropy increases with pressure for a normal material.

A more realistic approximation is to add a viscous stress:

$$p = \overline{p}(V, E) - \alpha \, \mathrm{d}V/\mathrm{d}t \,. \tag{12}$$

If the dependence on E can be neglected, eqs. (5) and (12) together become a differential equation for the density profile in the shock front:

$$\alpha D \, \mathrm{d}V/\mathrm{d}\xi = p_0 + m^2(V_0 - V) - \overline{p}(V) \,. \tag{13}$$

In case the E-dependence of eq. (12) cannot be neglected, eqs. (5), (6) and (12) provide a description of the profile.

The sign of the entropy change in eq. (11) is directly related to the propagation process. For the shock wave of Fig. 1, moving into stationary material ($u_0 = 0$):

$$D^2 = V_0^2(p_1 - p_0)/(V_0 - V_1) > V_0^2 |\mathrm{d}p/\mathrm{d}V|_{V_0} \equiv c_0^2 \tag{14}$$

provided $(\partial^2 p/\partial V^2)_S > 0$ at (p_0, V_0). The velocity of sound is defined as $c = V(-\partial p/\partial V)_S^{\frac{1}{2}}$. The identity between $(\partial p/\partial V)_S$ and $\mathrm{d}p/\mathrm{d}V$ on the Hugoniot at (p_0, V_0) is possible because isentrope and Hugoniot have a second-order contact at the foot of the Hugoniot. This will be discussed later by ROYCE and KEELER. The inequality in (14) tells us that the shock wave overtakes any acoustic wave ahead of it. Under the same conditions a disturbance behind the shock front overtakes the shock, provided, of course, that both

are travelling in the same direction. This can be seen in the following way: The propagation velocity of a forward-facing disturbance is $u_1 + c_1$; if $u_1 + c_1 > D$, the disturbance will overtake the shock. Equation (11) can be converted into a differential equation for the Hugoniot by assuming that $S = S(p, V)$ and proceeding to eliminate $\mathrm{d}S/\mathrm{d}p$. The result is:

$$\mathrm{d}p_1/\mathrm{d}V = \{(\partial p_1/\partial V_1)_S + \Gamma(p_1 - p_0)/2V_1\}/\{1 - \Gamma_1(V_0 - V_1)/2V_1\}\,, \tag{15}$$

where $\Gamma = V(\partial p/\partial T)_V/C_V$. It has already been shown that $-\mathrm{d}p/\mathrm{d}V > (p - p_0)/(V_0 - V)$ in Fig. 2, and this with eq. (15) leads to the inequality:

$$c_1^2/(D - u_1)^2 - \Gamma_1(V_0 - V_1)/2V_1 > 1 - (\Gamma_1/2V_1)(V_0 - V_1)\,. \tag{16}$$

Then $c_1^2 > (D - u_1)^2$ or

$$u_1 + c_1 > D_1\,, \tag{17}$$

provided the Rayleigh line is less steep than the tangent to the Hugoniot at (p_1, V_1). We say that in this case the flow behind the shock is *subsonic*. A single shock connecting (p_0, V_0) and (p_1, V_1) is accordingly stable. If $D_1 > u_1 + c_1$, then (p_1, V_1) is a point of instability and the possibility of forming a second shock exists [2].

Experimentally produced shock waves seldom exactly satisfy the requirements of steady flow assumed in deriving the jump conditions. The states connected by the shock transition may not be precisely uniform or the shock wave has not propagated far enough to become steady. However, the experimental conditions may be very close to the theoretical assumptions, and it is quite likely that errors involved in applying the jump conditions to experiments are less than those originating from other sources. Such errors may be significant if gradients in adjacent regions are comparable to those in the shock or if time has not been sufficient for the flow to become steady and the curvature of the Hugoniot is large. The resolution of this question is a constant source of concern to experimentalists and no satisfactory resolution has been made. BLAND [3] has considered the development of a step change in pressure for a viscous material and concludes that the shock profile is essentially steady after travelling a distance of five shock thicknesses from the source. This is an interesting result. The difficulty in applying it is that, in general, the steady shock thickness is unknown.

2. – Rarefactions and characteristics.

Referring to our original model of a pressure on a half-space, we suppose that after being held at constant value p_1 while the shock was being formed, we then reduce the pressure to its ambient value p_0. A forward-facing rare-

faction is produced, and we seek an appropriate method for describing the propagation of this rarefaction.

According to the discussion of Sect. 1, waves of rarefaction cannot be steady in the sense of eqs. (4)-(6) for normal materials; *i.e.*, there are no solutions of the form $\varrho = \varrho(x - Dt)$, etc., for constant D. We do know, however, that waves of infinitesimal amplitude satisfy the simple wave equation, and that solutions of this are in the form

$$f(x - ct) + g(x + ct) .$$

That is, they consist of forward-facing and backward-facing waves. For such infinitesimal waves we know that

$$\mathrm{d}p = \varrho c \, \mathrm{d}u \tag{18a}$$

for forward-facing waves and

$$\mathrm{d}p = -\varrho c \, \mathrm{d}u \tag{18b}$$

for backward-facing waves. Here c is the velocity with which these infinitesimal disturbances travel into material at rest. Equations (18) are in accord with the jump conditions if we apply them to waves of infinitesimal amplitude.

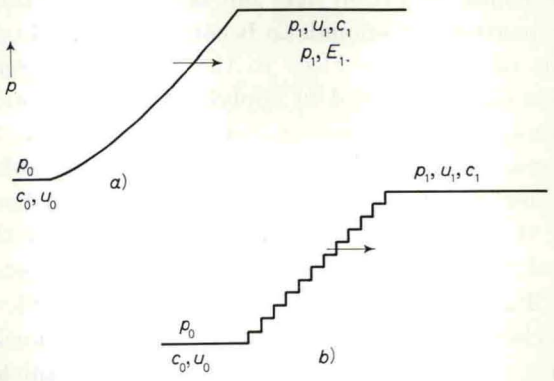

Fig. 3. – *a*) Continuous forward-facing rarefaction wave. The propagation velocity at each point is $u + c$. *b*) Representation of continuous rarefaction as sequence of small increments for which $\delta p = \varrho c \, \delta u$.

If we consider our forward-facing rarefaction to be represented by a sequence of jumps, $\mathrm{d}p$, to lower pressure, accompanied by a sequence of jumps, $\mathrm{d}u$, to smaller particle velocity, we can integrate eq. (18) to obtain the relation between p and u at any point in the rarefaction. This is illustrated in Fig. 3

and the result is

$$u - u_1 = \int_{p_1}^{p} \mathrm{d}p/\varrho c \,. \tag{19a}$$

The equivalent relation for backward-facing rarefactions is

$$u - u_1 = -\int_{p_1}^{p} \mathrm{d}p/\varrho c \,. \tag{19b}$$

Defining the new variable

$$l = \int^{p} \mathrm{d}p/\varrho c \,, \tag{20}$$

Equations (19) can be written

$$u - l = \text{const} = u_1 - l_1 \equiv -2s_1 \tag{21}$$

for forward-facing rarefactions, and

$$u + l = \text{const} = u_1 + l_1 = 2r_1 \tag{22}$$

for backward-facing ones. The constants r_1 and s_1 are called « Riemann invariants ».

To understand the implications of eqs. (21) and (22) more fully, consider the special case of isentropic flow, for which eq. (3) reduces to $\mathrm{d}S/\mathrm{d}t = 0$. Then eqs. (1) and (2) can be combined to form an equivalent set of « characteristic equations »:

$$[\partial/\partial t + (u + c)\,\partial/\partial x](u + l) = 0 \,, \tag{23}$$

$$[\partial/\partial t + (u - c)\,\partial/\partial x](u - l) = 0 \,. \tag{24}$$

The curves on which $\mathrm{d}x/\mathrm{d}t = u \pm c$ are called « characteristic curves »; eqs. (23) and (24) are thus equivalent to the set:

$$C+: \quad u + l = \text{const} = 2r\,; \qquad \mathrm{d}x/\mathrm{d}t = u + c \,, \tag{25}$$

$$C-: \quad u - l = \text{const} = -2s\,; \qquad \mathrm{d}x/\mathrm{d}t = u - c \,. \tag{26}$$

In words, r is constant on the $C+$ characteristic curves for which $\mathrm{d}x/\mathrm{d}t = u + c$; s is constant on the $C-$ characteristics. Equations (25) and (26) are

true when the flow is a mixture of forward- and backward-facing waves. For forward-facing waves, eq. (21) is also true; then

$$C+: \quad u + l = 2r, \tag{27}$$

$$C-: \quad u - l = 2s_1. \tag{28}$$

For backward-facing waves:

$$C+: \quad u + l = 2r_1, \tag{29}$$

$$C-: \quad u - l = -2s. \tag{30}$$

To summarize:

Forward-facing shock waves running into material with velocity u_0 and in the state (p_0, V_0) satisfy the relations

$$D - u_0 = V_0\sqrt{(p_1 - p_0)/(V_0 - V_1)}, \tag{31}$$

$$u_1 - u_0 = \sqrt{(p_1 - p_0)\,(V_0 - V_1)}. \tag{32}$$

Backward-facing shocks, the relations

$$D - u_0 = -V_0\sqrt{(p_1 - p_0)/(V_0 - V_1)}, \tag{33}$$

$$u_1 - u_0 = -\sqrt{(p_1 - p_0)\,(V_0 - V_1)}. \tag{34}$$

For forward-facing rarefactions running into material in the uniform state (p_0, V_0) with velocity u_0,

$$u - u_0 = l - l_0. \tag{35}$$

For backward-facing rarefactions moving into the same state,

$$u - u_0 = -(l - l_0). \tag{36}$$

For rarefactions there are no equations analogous to (31) and (33) because there is no single propagation velocity associated with a rarefaction. Waves for which eq. (35) or eq. (36) applies are called « simple waves ». In the general case of isentropic flow in which, for example, two rarefactions are interacting, eqs. (25) and (26) describe the flow.

In condensed materials compressed by shock waves to about 15 % of their initial volume or less, the shock wave is called « weak ». Then the entropy-

change is small and the shock can be treated as a simple wave to which either eq. (35) or (36) applies. In this approximation the interactions of shock waves and rarefactions can be calculated from eqs. (25) and (26).

3. – Elementary wave interactions.

Equations (32), (34), (35) and (36) uniquely define and limit the values of particle velocity, u, which can be achieved by simple shock or rarefaction from a given state (p_0, V_0, u_0). This limitation on states which can be reached in a single wave transition supplies a powerful tool for thinking about and calculating the fields of high-amplitude waves. The problem is transformed into a « hodograph » plane in which the variables are (u, p), (u, l), (r, s) or some equivalent set. We shall use u, p here because of continuity conditions on u and p at an interface or boundary. The significance of this choice will appear later.

Various useful representations of a shock and of a rarefaction are shown in Fig. 4. In 4 *a*) is a cross-section of a half-space to which a pressure p_1 was applied at $t = 0$ and released at $t = t_0$. The pressure profile at this particular $t > t_0$ is shown in 4 *b*). It consists of a forward-facing shock, designated $\mathscr{S}_+$, a region of uniform pressure p_1 and particle velocity u_1, and a rarefaction $\mathscr{R}_+$. The notations $\mathscr{S}$ and $\mathscr{R}$ are introduced here to denote shock and rarefaction waves, respectively. Forward-facing waves are denoted by the subscript « + », backward-facing by « — ». In Fig. 4 *c*) the flow is shown in the (x, t) plane. Region I is the uniform initial state (p_0, V_0, u_0) with $u_0 > 0$. The shock front, $\mathscr{S}_+$, has constant slope until the following rarefaction overtakes it, reducing its amplitude and velocity. Region II is the uniform state (p_1, u_1, V_1) behind the shock. Region III is the rarefaction $\mathscr{R}_+$ in which pressure and particle velocity are diminishing. Region IV is again at the ambient pressure p_0 but volume and particle velocity now differ from V_0 and u_0. The path OAB is the trace of the half-space surface, sometimes called the « piston path », $\mathscr{P}$. The dashed curve is the path of a single particle or mass element traversed successively by $\mathscr{S}_+$ and $\mathscr{R}_+$. Figure 4 *d*) shows the wave process in the (p, V) plane. The initial shock compression is along the Rayleigh line to the state B on the Hugoniot. The rarefaction, assumed to be isentropic, expands the material along the dashed isentrope to the final state $C(V_0', p_0, u_0')$. In Fig. 4 *e*) the process is shown in the (p, u) plane. The straight line AB with slope $\mathrm{d}p/\mathrm{d}u = \varrho_0(D - u_0)$ is the image of the Rayleigh line. The compressed state B lies on the image of the Hugoniot curve and the dashed curve BC is the image of the isentrope of Fig. 4 *d*). Because the shock process is entropic and because most materials have positive thermal expansion coefficients, the final state (u_0', p_0) is normally to the left of (u_0, p_0) for forward-facing waves.

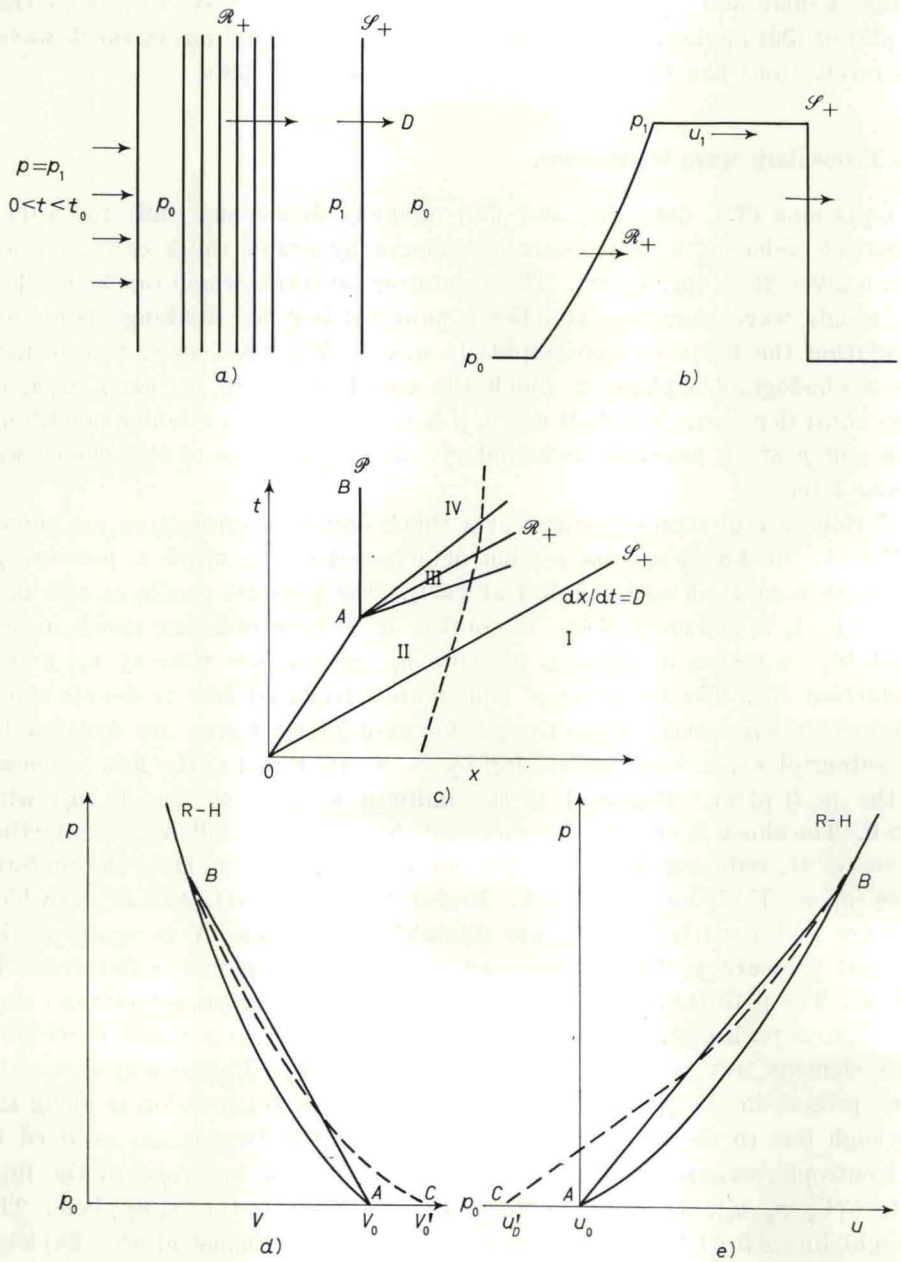

Fig. 4. – Forward-facing rarefaction overtaking a shock. *a*) planes of constant phase in half-space; *b*) pressure profile, $t > t_0$; *c*) (x-t) diagram; *d*) (p-V) diagram; *e*) (p u)-plane.

A set of similar figures can be drawn for backward-facing waves. Figure 4 *d*) is then unchanged. The others are produced by reflection in the vertical axis, except that appropriate adjustments need to be made depending upon the magnitude and sign of u_0.

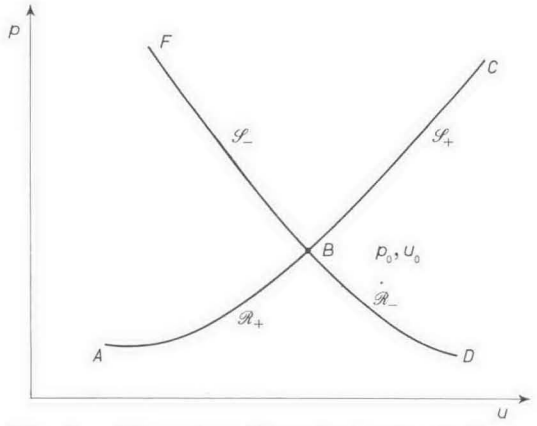

Fig. 5. – Wave transitions in the (p, u) plane.

The essential point of the following discussion is that states connected by shocks or by simple waves to an arbitrary state (p_0, u_0) must lie on fixed curves given by eqs. (32), (34), (35), (36), provided there are no time-dependent terms in the constitutive relations. This is illustrated in Fig. 5. *AB* is represented by eq. (35), *BC* by (32), *BF* by (34) and *BD* by (36). *AB* and *BC* have a second-order contact at *B*, arising from the second order contact between isentrope and Hugoniot at the initial state (p_0, V_0). So do *BD* and *BF*.

Some applications of the foregoing principles are illustrated in Fig. 6-13.

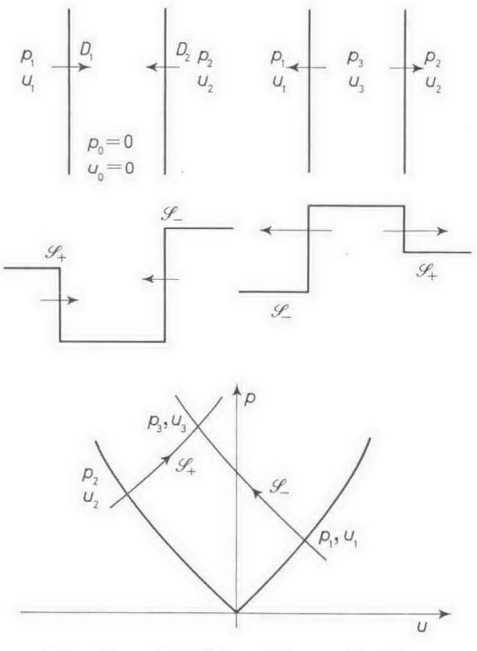

Fig. 6. – Collision of two shocks.

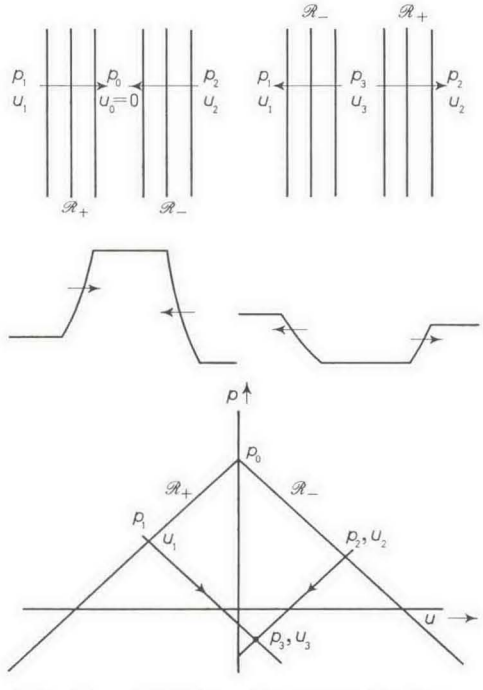

Fig. 7. – Collision of two rarefactions.

Figure 6: Two shocks approach one another, separated by a uniform state $p_0 = 0 = u_0$. They are represented by the points (p_1, u_1) and (p_2, u_2) in the (p, u) plane. After collision there are two waves drawing apart, separated by a new state (p_3, u_3) and running into the uniform states (p_1, u_1) and (p_2, u_2), respectively. The transition from (p_2, u_2) to (p_3, u_3) occurs across a forward-facing wave, that from (p_1, u_1) across a backward-facing wave. The state between the separating waves must be uniform in (p, u) because of continuity conditions on p and u. All these conditions are satisfied by the intersection of the $\mathscr{S}_-$ and $\mathscr{S}_+$ curves from (p_1, u_1) and (p_2, u_2), respectively.

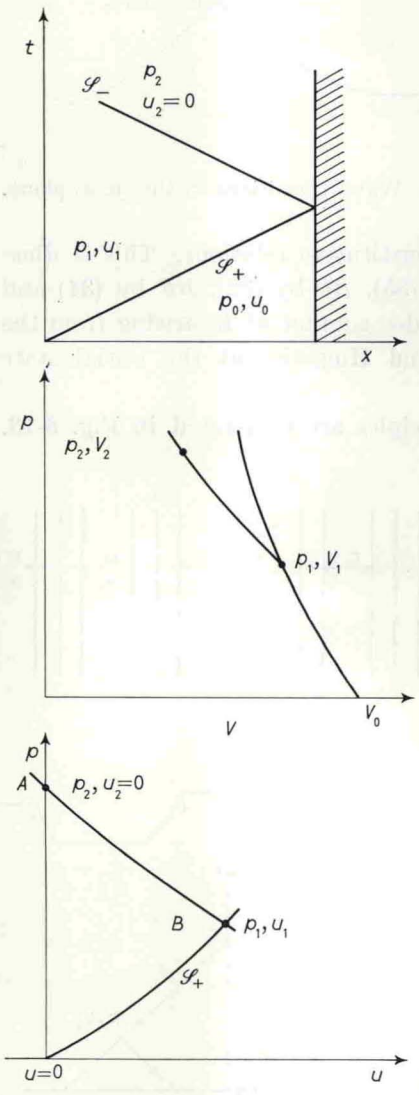

Fig. 8. – Reflection of a uniform shock at a rigid wall. $p_2/p_1 > 2$ if $d^2p/dV^2 > 0$.

Figure 7: Collision of two rarefactions: The argument is analogous to the previous one. The initial state p_0, $u_0 = 0$, is connected by rarefactions to (p_1, u_1) and (p_2, u_2). The final state reached from (p_1, u_1) and (p_2, u_2) must lie at the intersection of wave transition curves passing through these states and must be a state of uniform p and u. This is satisfied by (p_3, u_3).

Figure 8: Reflection of a uniform shock at a rigid wall: The initial shock, $\mathscr{S}_+$, carries material from $(u_0 = 0 = p_0)$ to (p_1, u_1). After reflection the state (p_1, u_1) is connected to the final state $(p_2, u_2 = 0)$ by a backward-facing wave. The final state must lie on the curve for backward-facing transitions in the (p, u) plane and also on the $u = 0$ axis. These conditions are satisfied at point A. Note particularly that if the $\mathscr{S}_+$ curve is concave upward in the (p, u) plane, $p_2 > 2p_1$. The $\mathscr{S}_-$ curve through B is the mirror image of the $\mathscr{S}_+$ curve in a vertical axis through B.

Figure 9: Reflection of a uniform shock at a free surface: This is similar to the preceding, but the final state must now lie on the $p = 0$ axis. For condensed

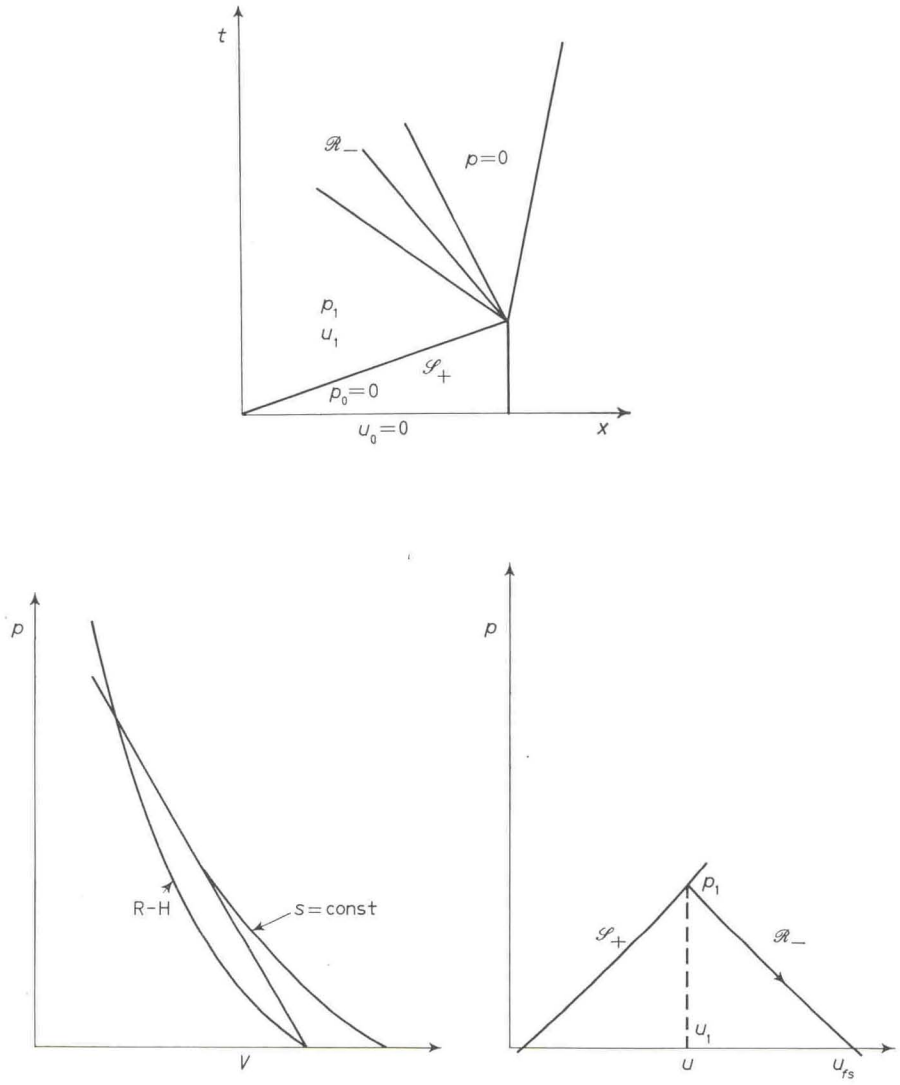

Fig. 9. – Uniform shock on a free surface.

material, u_{fs} is approximately equal to and usually slightly greater than $2u_p$.

Figure 10: Transmission of a uniform shock through an interface: The shock is incident from material I on material II. The (p, u) curves labelled I and II are images of the Hugoniot (p, V) curves of the respective materials. The final state (p_2, u_2) is common to both materials since p_2 and u_2 are to be continuous across the interface. This final state must be reached from (p_1, u_1)

by a backward-facing wave in material I and from ($p_0 = 0 = u_0$) by a forward-facing wave in II. The required state is as shown. Material II was arbitrarily chosen so that its Hugoniot image lies above I. In that case the wave reflected back into I is a shock wave. For II below I, the reflected wave is a rarefaction. It sometimes happens that the two curves cross; then the reflected wave is a shock or a rarefaction, depending on the amplitude of the incident shock. For an incident shock at the intersection there is no reflection. An analytic expression for the amplitude of a reflected shock can readily be obtained from the jump conditions written for the incident shock, the reflected shock, and the transmitted shock:

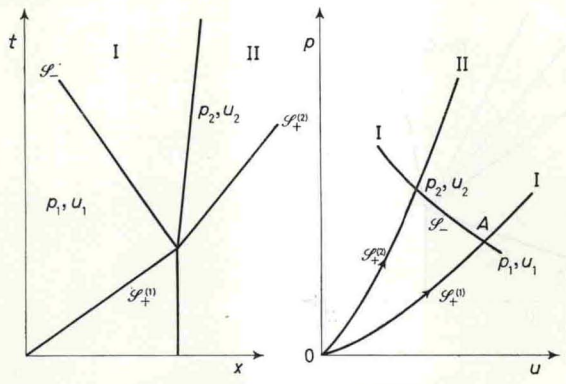

Fig. 10. – Transmission through an interface; $\varrho_{02} D_2 > \varrho_{01} D_1$.

$$\frac{p_2 - p_0}{p_1 - p_0} = \frac{1 + \varrho_0 D_1/\varrho_1 D'_{21}}{\varrho_0 D_1/\varrho_1 D'_{21} + \varrho_0 D_1/\varrho'_0 D_2}, \tag{37}$$

where

ϱ_0 = initial density of material I,

ϱ'_0 = initial density of material II,

D_1 = velocity of incident shock,

D'_{21} = velocity of reflected shock *relative to the material ahead* $= u_1 - D_{21}$,

D_{21} = velocity of reflected shock in laboratory co-ordinates,

D_2 = velocity of transmitted shock,

ϱ_1 = density behind initial shock.

The products ϱD appearing in eq. (37) are *shock impedances* corresponding to the various waves. Shock impedance for a given transition is equal to the magnitude of the slope of the corresponding chord in the (p, u) plane. For example, $\varrho_0 D_1$ is the slope of the chord OA in Fig. 10. In the limit of small amplitude waves, the shock impedance becomes equal to the acoustic impedance. Then eq. (37) reduces to the expression for acoustic reflection:

$$(p_2 - p_0)/(p_1 - p_0) = \delta p_2/\delta p_1 = 2\varrho'_0 c'_0/(\varrho_0 c_0 + \varrho'_0 c'_0). \tag{38}$$

For a rigid wall $\varrho_0' D_2 \to \infty$ and eq. (37) becomes

$$\frac{p_2 - p_0}{p_1 - p_0} = \frac{\varrho_1 D_{21}' + \varrho_0 D_1}{\varrho_0 D_1} \xrightarrow[p_1 \to p_0]{} 2 \,. \tag{39}$$

For a free surface, $\varrho_0' D_2 = 0$ and eq. (37) becomes

$$(p_2 - p_0)/(p_1 - p_0) = 0 \,. \tag{40}$$

Equation (37) applies exactly only when the reflected wave is a shock. Because of the second-order contact between the rarefaction branch and the shock branch of the cross curve passing through A, the formula provides a very good approximation for rarefactions in condensed materials.

Figure 11: Weak-shock approximation: Equations (32) and (35) yield very nearly the same curve when $(V_0 - V)/V_0 \leqslant 0.15$. Then either can be used and the (p, u) plane can be mapped with a set of identical curves and their mirror images. These curves can be regarded as transformations from the (x, t) plane. A curve along which transitions can be made by forward-facing waves is an image of a $C-$ characteristic and is called a Γ_- characteristic.

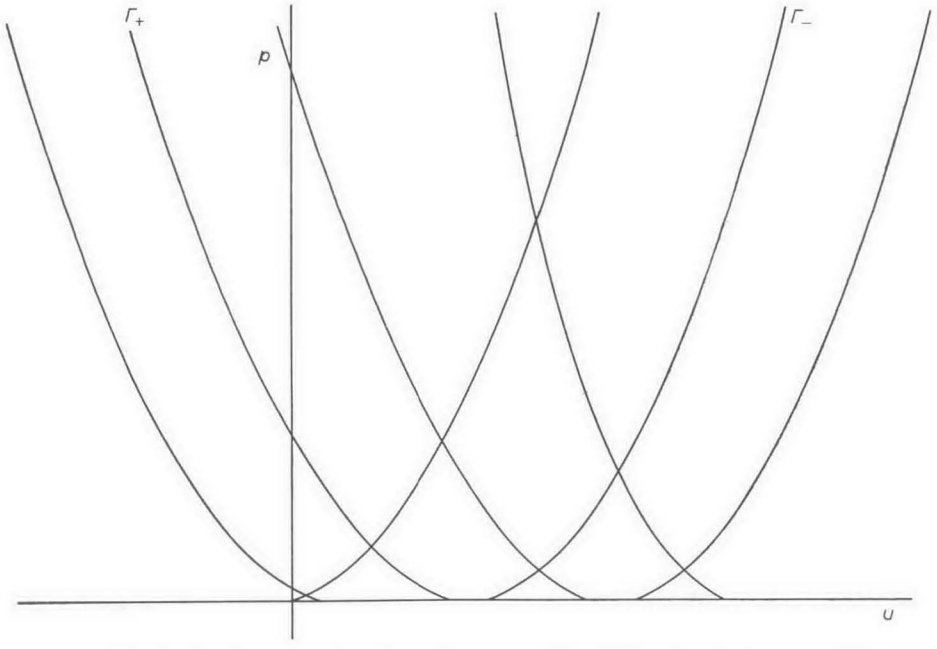

Fig. 11. – Weak shock approximation, $S = \text{const}$. No distinction between adiabat and Hugoniot; $(p\text{-}u)$ plane can be mapped with images of the $C+$ and $C-$ characteristics. $u - l = \text{const}$ on Γ_-, $u + l = \text{const}$ on Γ_+.

Transitions through backward-facing waves are along Γ_+ characteristics. Transformation from the (x, t) to the (x, u) plane is not necessarily one-one. For example, a region of uniform state in the (x, t) plane maps into a single point in the (p, u) plane; a simple wave in the (x, t) plane maps into one of the Γ characteristics.

An example of application of the characteristic mapping of the (p, u) plane in the weak shock approximation is shown in Fig. 12. A forward-facing rarefaction travels into a uniform state $(p_0, u_0 = 0)$ bounded by a rigid wall, reducing it to the uniform state (p_1, u_1). The reflection process is represented in the (x, t) plane by drawing $C+$ and $C-$ characteristics at arbitrarily close intervals and labelling the fields between the characteristics as shown. In relating this flow to the (p, u) plane, each field in the (x, t) plane is considered a region of uniform state, represented by a single point in the (p, u) plane. Thus the regions 00, 01, 02, 03 map into the points 00, 01, 02, 03 on the Γ_- characteristic $(u - l = l_0)$ passing through $(p_0, u_0 = 0)$. Region 11 in (x, t) is reached from 01 across a backward-facing wave, therefore it lies on a Γ_+ characteristic passing through 01. The rigid boundary condition $u = 0$ must be satisfied in 11, therefore 11 in (p, u) lies at the intersection of the Γ_+ through 01 and the $u = 0$ axis. Similarly the transition from 02 to 12 to 22 takes place along a Γ_+ characteristic and terminates at $u = 0$. The intermediate state 12 is reached via a backward-facing wave from 02 and a forward-facing wave from 11, etc. This simple step by step procedure will succeed in unraveling the most complicated flow problems in (x, t) geometry provided only that the weak shock approximation is valid. With the aid of a large drawing board and considerable patience, the procedure is useful for graphical computation; and the solution of a few problems by this means is certain to establish the elements of finite amplitude wave propagation firmly in the mind of the student. It should be noted that the C characteristics are actually curved in the region of interaction, and the slopes of those characteristics

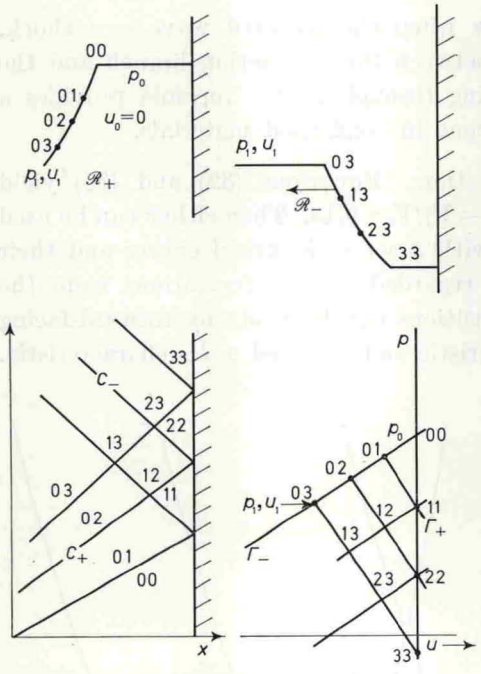

Fig. 12. – Rarefaction on a rigid wall.

bounding the fields 11, etc., are determined from the values of p and u at the intersections of the corresponding Γ characteristics.

A further application of the weak shock approximation is shown in Fig. 13, where a common experimental problem is described in the (x, t) and (p, u) planes. A pressure-free flyer plate with uniform velocity w collides at $t = 0$ with a stationary pressure-free target, producing shock waves which travel forward into the target and backward into the flyer. The shock in the flyer reflects from the back face as a rarefaction, and there is subsequently a succession of reflections between free surface and interface which ultimately bring the flyer to a stop. The sequence of states, preserving continuity of u and p, is shown in the figure. The time between reflections is twice the travel time through the flyer, so the time to effectively stop the flyer can be estimated.

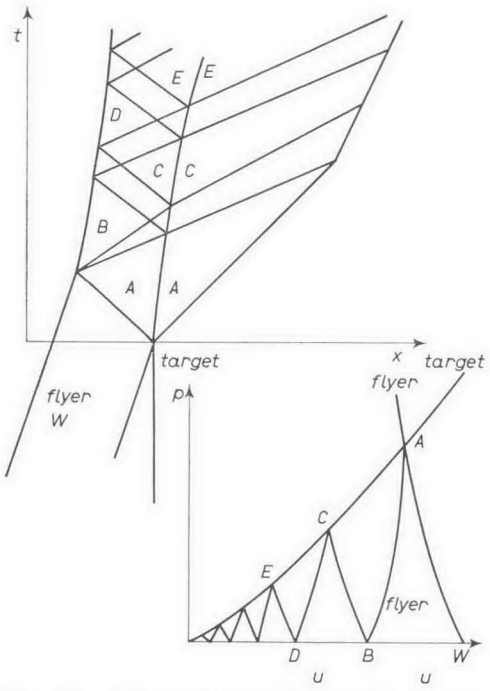

Fig. 13. – Flyer plate colliding with target.

4. – Elastic-plastic solids.

Much of the material in the preceding Sections has been couched in the language of fluids, though it applies equally well to solids, and has made but little reference to the explicit material properties involved. In this Section we become more specific about materials and examine more explicitly propagation effects in these models.

It must be recognized at the outset that there are no physically complete descriptions of the thermomechanical properties of solids. Hooke's law of elasticity is commonly used for small strains in metals and brittle solids, though there are materials to which it does not apply. Some materials are viscoelastic even at small strains, and the proper description of such materials is subject to current research. All solids fail through flow or fracture at some stress, and above this level, Hooke's law is totally improper. A satisfactory theory of fracture is far from realization; and the theory of plastic failure, while far advanced compared to fracture, is still logically incomplete

and is often at odds with experimental results. However, the theory of plasticity is more completely formulated than other models of anelasticity, and its applications in shock propagation will be discussed here.

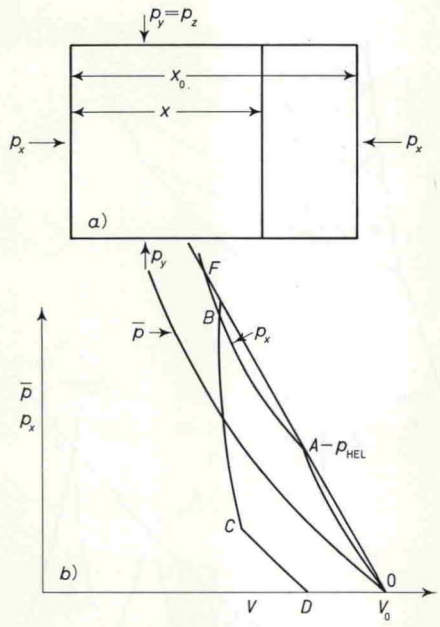

Fig. 14. – *a*) A parallelepiped of initial length x_0 has been compressed uniaxially to length x. *b*) Stress-strain relations for the sample of Fig. 14 *a*).

We restrict ourselves to the case of uniaxial strain existing in plane shock waves. We suppose a small element of volume to be compressed in the x-direction only and consider the relations between stress and strain. The notation used is shown in Fig. 14 *a*) and the expected stress-strain relation in a cycle of compression and rarefaction is shown in Fig. 14 *b*). Principal coordinates of the stress and strain matrices are (x, y, z) with x the direction of shock wave propagation. In order to maintain the condition of uniaxial strain while p_x is applied, p_y and p_z must be adjusted so as to maintain the lateral dimensions unchanged. Symmetry requires that $p_y = p_z$.

The most common assumptions of elasto-plasticity are:

i) Material response is elastic as long as deformation stresses do not exceed a characteristic value. The most commonly used criterion of failure is the von Mises condition

$$(41a) \qquad (p_x - p_y)^2 + (p_x - p_z)^2 + (p_y - p_z)^2 \leqslant 2Y^2 ,$$

where Y is the yield stress in simple tension. In uniaxial strain this becomes

$$(41b) \qquad |p_x - p_y| \leqslant Y .$$

If the inequality applies, the material is elastic and satisfies Hooke's law:

$$(42a) \qquad p_x = \lambda\theta + 2\mu\varepsilon_x ,$$

$$(42b) \qquad p_y = \lambda\theta + 2\mu\varepsilon_y ,$$

$$(42c) \qquad p_z = \lambda\theta + 2\mu\varepsilon_z ,$$

where $\theta = \varepsilon_x + \varepsilon_y + \varepsilon_z$. In uniaxial strain, $\varepsilon_x = (V_0 - V)/V_0$, $\varepsilon_y = \varepsilon_z = 0$. If the equality holds, the material is in the plastic state.

ii) In the plastic state, every increment in strain is the sum of an elastic and a plastic increment:

$$\mathrm{d}\varepsilon_x = \mathrm{d}\varepsilon_x^e + \mathrm{d}\varepsilon_x^p \,, \tag{43a}$$

$$\mathrm{d}\varepsilon_y = \mathrm{d}\varepsilon_y^e + \mathrm{d}\varepsilon_y^p \,, \tag{43b}$$

$$\mathrm{d}\varepsilon_z = \mathrm{d}\varepsilon_z^e + \mathrm{d}\varepsilon_z^p \,. \tag{43c}$$

iii) There is no plastic dilatation:

$$\mathrm{d}\varepsilon_x^p + \mathrm{d}\varepsilon_y^p + \mathrm{d}\varepsilon_z^p = 0 \,. \tag{44}$$

iv) The stress is supported solely by the elastic strain:

$$\mathrm{d}p_x = \lambda\,\mathrm{d}\theta + 2\mu\,\mathrm{d}\varepsilon_x^e \,, \tag{45a}$$

$$\mathrm{d}p_y = \lambda\,\mathrm{d}\theta + 2\mu\,\mathrm{d}\varepsilon_y^e \,, \tag{45b}$$

$$\mathrm{d}p_z = \lambda\,\mathrm{d}\theta + 2\mu\,\mathrm{d}\varepsilon_z^e \,, \tag{45c}$$

where λ and μ are, in general, functions of the density.

As p_x is increased from zero, the response is initially elastic and $\varepsilon_y = \varepsilon_z = 0$. Then

$$p_x - p_y = (1-2\nu)p_x/(1-\nu) \,, \tag{46}$$

where $\nu = \lambda/2(\lambda+\mu)$ is Poisson's ratio. The yield stress is reached at a value of p_x called the « Hugoniot elastic limit », denoted by p_{HEL}. From eqs. (41) and (46):

$$p_{\mathrm{HEL}} = (1-\nu)\,Y/(1-2\nu) \,. \tag{47}$$

For further increases in p_x, the material is in the plastic state. Then

$$p_x \equiv \overline{p} + \tfrac{2}{3}(p_x - p_y) = \overline{p} + 2Y/3 \,, \tag{48}$$

where $\overline{p} = (p_x + p_y + p_z)/3$, a function of density and internal energy alone. Referring to Fig. 14 *b*), eq. (48) applies to the segment AB of the p_x curve. The slope of the (p_x, V) curve in the elastic region is, from eqs. (42):

$$\mathrm{d}p_x/\mathrm{d}V = -(\lambda + 2\mu)/V_0 = -(K + 4\mu/3)/V_0 \,, \tag{49}$$

where K is bulk modulus. In the plastic region, AB, the slope is, for constant Y, from eq. (48)

$$\mathrm{d}p_x/\mathrm{d}V = \mathrm{d}\bar{p}/\mathrm{d}V = -K/V. \tag{50}$$

In accord with eq. (50), it is convenient to define the incremental dilatation as $\mathrm{d}V/V$. Bulk modulus normally increases with $\bar{p}$, so AB is normally concave upward. The yield stress, Y, is in general a function of plastic work and density. In such case eq. (50) is augmented by a $\mathrm{d}Y/\mathrm{d}V$ term. In any case the offset of p_x from the hydrostat, $\bar{p}$, is always $2Y/3$.

At point B in Fig. 14 *b*) we suppose that a change is made from monotonically increasing to monotonically decreasing p_x. Equation (41) must again be examined to determine whether the mass element is in the elastic or plastic state. During the initial compression process, p_x increased more rapidly than p_y until yield occurred. During unloading, p_x decreases more rapidly than p_y until yielding again occurs. Thus the portion BC of the unloading curve is elastic until $p_y - p_x = Y$ at C. From C to D, unloading is plastic and the unloading curve lies below the hydrostat by $\frac{2}{3}Y$.

Referring to the discussion following eq. (17), we see that point A of Fig. 14 *b*) may be a point of instability for single shock compressions. To see that this is indeed the case, suppose that a shock wave has been generated with amplitude p_{HEL}, traveling with speed

$$D_E = [V_0(\lambda + 2\mu)]^{\frac{1}{2}}.$$

The velocity of this shock front relative to the material behind it is

$$D_e - u_E = (V_A/V_0)D_E = V_A\sqrt{(\lambda + 2\mu)/V_0}. \tag{51}$$

If an additional compression of small amplitude is produced to follow the already established shock, it will travel with velocity c_A relative to the material ahead of it, where, according to eq. (50),

$$c_A = \sqrt{KV_A} = V_A\sqrt{(\lambda + 2\mu/3)/V_A}.$$

Comparing this with eq. (51) we find that

$$(D_E - u_E)^2/c_A^2 = (3V_A/V_0)(1-\nu)/(1+\nu) \simeq 3(1-\nu)/(1+\nu) = \tfrac{3}{2} \quad \text{for } \nu = \tfrac{1}{3}, \tag{52}$$

since $V_A/V_0 \simeq 1$ at the Hugoniot elastic limit. According to eq. (52), the second wave does not overtake the shock, so there is a region of the (p_x, V) curve above the point A which cannot be reached by a single shock from

(p_0, V_0). This region, AF in Fig. 14 *b*), is defined by extending the Rayleigh line OA until it intersects the Hugoniot AB at the point F. Pressures in this region will be reached by a double shock, illustrated in Fig. 15. The first

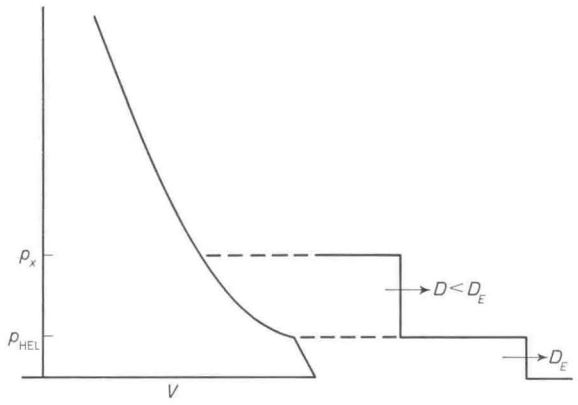

Fig. 15. – Double shock in elastic-plastic material.

shock is called the « elastic precursor »; it travels with elastic velocity, and its amplitude is p_{HEL}.

The unloading wave following an elastic-plastic shock also consists of two waves, but these are not always clearly distinguishable because of the spreading of the rarefactions. The decay process for an elastic-plastic shock is accelerated, however, by an elastic wave running back and forth between the shock front and the plastic rarefaction [4].

An example of an elastic-plastic shock in aluminum is shown in Fig. 16.

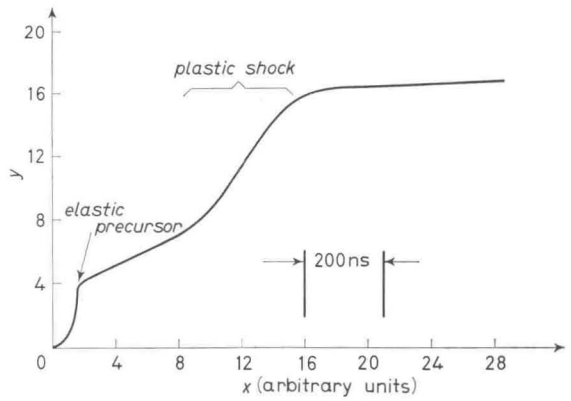

Fig. 16. – Shot no. 68-015. 6061-T6 Al target $\frac{1}{2}$ in. thick, recorded with 1 $\frac{1}{4}$ in. quartz gauge in Graham configuration. Peak pressure: 19 kb. Elastic precursor: 5.2 kb. (R. Mitchell, W.S.U.).

This record was obtained with a quartz gauge on the surface of a 6061-T6 Al target struck by a half-inch thick plate of the same material. The elastic precursor and plastic shock are readily distinguished.

A number of experiments on wave shape and shock decay have established that in aluminum, at least, and probably in other metals as well, the elastic-plastic model is substantially correct, though there are significant deviations due probably to Bauschinger effect and stress relaxation [5].

5. – Solid-solid phase transitions.

Another source of instability in shock waves is the solid-solid phase transition. A schematic diagram of a first-order transition in the (p, V) plane is shown in Fig. 17. An isotherm crosses the mixed phase region at constant pressure; an adiabat has, typically, a small negative slope. The change in slope of the adiabat on crossing the phase boundary can be readily calculated by straightforward application of thermodynamics [6]. In terms of sound velocity in phase 1, c_1, and equilibrium sound velocity in mixed phase, c_m, the change of slope is given by

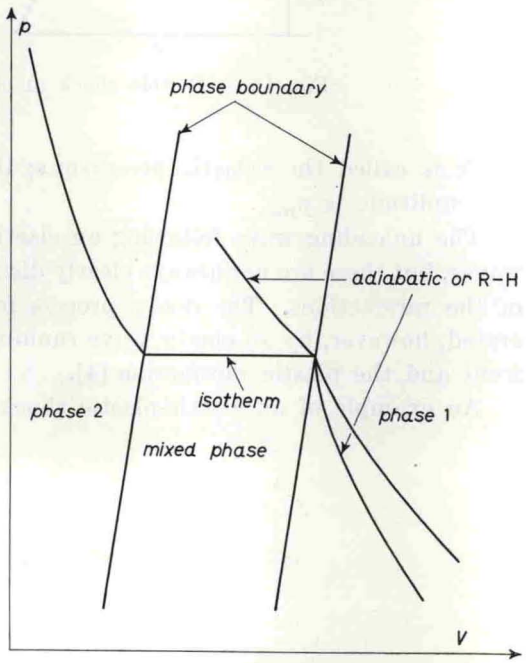

Fig. 17. – Reversible transition.

$$(53) \qquad (c_1^2 - c_m^2)/c_1^2 c_m^2 = \\ = (C_p/V^2 T)[(\partial T/\partial p)_s - \mathrm{d}T/\mathrm{d}p]^2 ,$$

where all quantities are evaluated at the phase boundary. Numerical computations for iron and bismuth show that the mixed phase adiabat is almost flat. Since the Hugoniot for the second shock and the mixed phase adiabat have a second order contact at the phase boundary, the Hugoniot is similarly flat.

In preparing a formal representation of a set of constitutive relations for use with the flow equations, eqs. (1)-(3), it is useful to keep in mind their mode of application. The most widely used procedure for integrating the flow equations is a staggered-difference scheme developed by VON NEUMANN and

RICHTMYER [7] in which time is advanced in increments of ΔT, and at each new time the positions, velocities, pressures, densities and energies of all the mass elements are computed. With this procedure in mind, we suppose that at a given point in the mixed phase region all the thermodynamic quantities are known and we then advance specific volume by a small amount $\mathrm{d}V$ and compute the other thermodynamic variables anew.

In an equilibrium phase change we assume that p and T are common to both phases and that extensive variables are given by a mass-weighted average over the two phases; *i.e.*, for example:

$$V = V_1(1-f) + V_2 f, \tag{54}$$

$$E = E_1(1-f) + E_2 f, \text{ etc.}, \tag{55}$$

where f is the mass fraction of material in phase 2. We now suppose that $V \to V+\Delta V$ and consequently $p \to p+\Delta p$, $f \to f+\Delta f$, $E \to E+\Delta E$, $T \to T+\Delta T$, etc., and proceed to calculate Δp, ΔT, ΔE and Δf. We must first of all assume that the equation of state is known for each phase individually, and it is most convenient to assume equations of state in the form

$$V_i = V_i(p, T), \tag{56a}$$

$$E_i = E_i(p, T). \tag{56b}$$

$$i = 1, 2,$$

Equations (54)-(56) are now differentiated with the intent of expressing $\mathrm{d}V$ and $\mathrm{d}E$ in terms of $\mathrm{d}p$, $\mathrm{d}T$, and $\mathrm{d}f$ with coefficients that depend on p, T, f. The result is

$$\mathrm{d}V = l_1 \mathrm{d}p + m_1 \mathrm{d}T + n_1 \mathrm{d}f, \tag{57}$$

$$\mathrm{d}E = l_2 \mathrm{d}p + m_2 \mathrm{d}T + n_2 \mathrm{d}f, \tag{58}$$

where

$$l_1 = (1-f)V_{1,p} + fV_{2,p}, \tag{59a}$$

$$l_2 = -(1-f)(TV_{1,T} + pV_{1,p}) - f(TV_{2,T} + pV_{2,p}), \tag{59b}$$

$$m_1 = (1-f)V_{1,T} + fV_{2,T}, \tag{59c}$$

$$m_2 = (1-f)(C_{p1} - pV_{1,T}) + f(C_{p2} - pV_{2,T}), \tag{59d}$$

$$n_1 = V_2 - V_1,$$

$$n_2 = E_2 - E_1,$$

$$V_{1,T} \equiv (\partial V_1/\partial T)_p, \qquad V_{2,p} \equiv (\partial V_2/\partial p)_T, \quad \text{etc.},$$

$$C_{p1} = \text{specific heat at constant pressure for phase 1, etc.}$$

There is an additional relation between dE and dV, *viz.* the first law. If there is no heat transfer,

$$dE = -(p+q)\,dV, \tag{60}$$

where q represents any irreversible forces in the compression process. Equations (57), (58) and (60) can now be solved for dp and dT:

$$dp = a_1\,dV + a_2\,df, \tag{61}$$

$$dT = b_1\,dV + b_2\,df, \tag{62}$$

where

$$a_1 = [m_2 + m_1(p+q)]/D, \tag{63a}$$

$$a_2 = (m_1 n_2 - m_2 n_1)/D, \tag{63b}$$

$$b_1 = -[l_2 + l_1(p+q)]/D, \tag{63c}$$

$$b_2 = (l_2 n_1 - l_1 n_2)/D, \tag{63d}$$

$$D = l_1 m_2 - l_2 m_1. \tag{63e}$$

It's clear from eqs. (61) and (62) that, since only dV is given, one more relation is required before dp and dT can be computed. For reversible transitions this is the Clausius-Clapeyron relation:

$$dp/dT = \Delta S/\Delta V = \text{fcn. of } p \text{ or } T. \tag{64}$$

Combining eqs. (61), (62) and (64) yields

$$df = \chi(p, T, V, f)\,dV. \tag{65}$$

This equation, together with eqs. (61) and (62), makes it possible to determine dp and dT. When that is accomplished, another increment, dV, is taken and the process is continued until the mass element enters the single phase region.

The above relations are also useful for computing the Hugoniot directly. To do this, replace eq. (60) by the differential form of the Rankine-Hugoniot equation and continue as before. To determine an isentrope, set $q = 0$ in eq. (60).

We have seen in Sect. 4 how the cusp in the (p, V) compression curve gives rise to a double wave: the elastic precursor followed by a plastic shock. The cusp at the phase boundary, shown in Fig. 17, is also a point of instability

which splits a shock to higher pressure into two. In fact, if the material undergoing a phase change is also elastic-plastic, a three wave structure may be produced, as in iron, illustrated in Fig. 18.

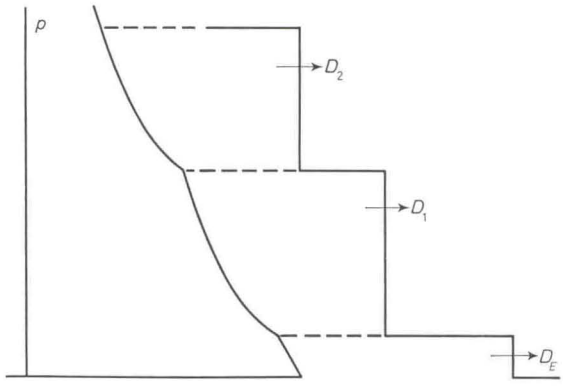

Fig. 18. – Three-wave structure in iron.

The phase transition is also responsible for a new phenomenon, the rarefaction shock. The unloading curve for an elastic-plastic material is always concave upward, the condition required for a rarefaction to spread as it progresses. But the unloading curve for an equilibrium phase transition of the kind shown in Fig. 17 has a convex upward region and this is responsible for producing a rarefaction shock. This is illustrated in Fig. 19.

The unloading curve is shown in Fig. 19 *a*) with two cusps, one at B and one at D. Suppose the material has been uniformly shocked to point $C(u_2, p_2)$,

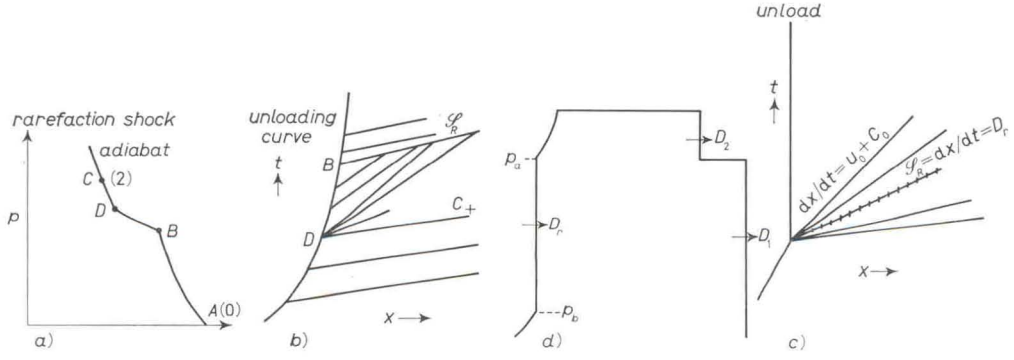

Fig. 19. – Rarefaction shock.

and that the pressure on the driving surface is slowly reduced so that the trace of the surface in the (x, t) plane is the curve BD shown in Fig. 19 *b*). At each decrement in driving pressure the free surface can be thought to send out a disturbance traveling along a $C+$ characteristic with velocity $u + c$. When the unloading process has progressed until the surface pressure has decreased from C to D, a singularity in the sound velocity c is encountered. At D we suppose c to take on all values from the second phase value on CD at D to the mixed phase value on DB at D. Then the point D on the unloading curve

in Fig. 19 *b*) is the source of a fan of $C+$ characteristics as shown. The slower sound velocities correspond to the steeper lines. From D to B the sound velocities are all small and the $C+$ characteristics are steep. At B a second singularity in c is encountered, but now the characteristics, instead of forming a fan as at D, crowd into one another, intersecting one another, and ultimately intersecting some of the characteristics from D. An intersection of two characteristics means that the field variables carried along the characteristics are multiple-valued at that point. In Fig. 19 *b*) the build-up of shock amplitude occurs over some distance as more and more characteristics intersect. In Fig. 19 *c*) we suppose that the driving pressure is released suddenly and the fully developed shock, $\mathscr{S}_R$, radiates from the corner in the unloading path as shown. In Fig. 19 *d*) is shown schematically the structure of a wave including a double compression shock and a rarefaction shock. The pressures p_a and p_b are determined by the condition that

$$(u+c)_a = D_R = (u+c)_b \,, \tag{65}$$

where D_R is the velocity of the rarefaction shock.

Some mechanical effects of the rarefaction shock will be described in Sect. 8.

6. – Stress-relaxation in elastic-plastic solids.

In order to provide a suitable framework for discussing the constitutive relations for a stress-relaxing solid, it is necessary to introduce some general concepts from continuum mechanics. We consider again an element of mass in a flow field, subject to forces of acceleration and compression transmitted through its immediate neighbors. We are interested in the response of this mass element to the stresses transmitted across its boundaries, and in order to discuss them we choose a co-ordinate system (x_1, x_2, x_3) which diagonalizes the stress and strain matrices. The principal stresses and strains are $\{\sigma_i\}$ and $\{\varepsilon_i\}$ respectively, with $i = 1, 2, 3$. We define a set of « stress deviators », S_i, and « strain deviators », E_i:

$$S_i = \sigma_i + \overline{p} \,, \tag{66}$$

$$E_i = \varepsilon_i - \theta/3 \,, \tag{67}$$

where $\overline{p} = -(\sigma_1 + \sigma_2 + \sigma_3)/3$, $\theta = \varepsilon_1 + \varepsilon_2 + \varepsilon_3$.

The S_i incorporate all the stress of deformation; the E_i are the strains of deformation. For purely elastic strain we can write Hooke's law in incre-

mental form:

$$d\sigma_i = \lambda\, d\theta + 2\mu\, d\varepsilon_i \,. \tag{68}$$

The definitions of S_i, E_i, p and θ lead to a restatement of Hooke's law as two equations:

$$d\bar{p} = -K\, d\theta \,, \tag{69}$$

$$dS_i = 2\mu\, dE_i \,. \tag{70}$$

In this form we separate those stresses which produce deformation from those which merely alter density so that the two relations can be discussed independently. It is commonly assumed that when nonelastic behavior occurs, it will appear in the deviator relation, not in hydrostatic compression. A notable exception is the porous solid, but that is not considered here. Following common practice we can write the constitutive relations for an elastic-plastic solid as:

$$dE_i = dE_i^e + dE_i^p \,, \tag{71}$$

$$dS_i = 2\mu\, dE_i^e \,, \tag{72}$$

$$d\bar{p} = -K\, d\theta \,, \tag{73}$$

where E_i^e and E_i^p are the elastic and plastic components of the strain deviator, respectively.

For a viscoelastic-plastic material, eqs. (71) and (73) apply as before, but (72) is replaced by

$$dS_i = 2\mu\, dE_i^e + 2\eta\, d\dot{E}_i^p \,, \tag{74}$$

where the dot indicates convective derivative with respect to time.

For a stress-relaxing solid we make the assumption that the plastic strain increment, in response to a change in stress, does not take its final value immediately. Its change is inhibited by a relaxation mechanism, undefined at this point. This process is represented by a relation of the form

$$dE_i^p/dt = F_i(S_i, \varrho)/2 \,. \tag{75}$$

The right-hand side of eq. (75) depends upon the amount by which E_i^p differs from its equilibrium value. Combining eqs. (71), (72) and (75) we arrive at the relation

$$dE_i/dt - (1/2\mu)\, dS_i/dt = F_i(S_i, \bar{p})/2 \,. \tag{76}$$

Equations (76) and (73) comprise a set of constitutive relations for a stress-relaxing material. Note particularly that the stress deviator, S_i, is entirely supported by the elastic strain, eq. (72). This distinguishes it fundamentally from the viscoelastic solid, eq. (74). Equations (71)-(73) for the elastic-plastic solid and eqs. (71), (73), and (76) for the elastic-plastic relaxing solid must be supplemented by a yield condition, *e.g.* the von Mises condition, eq. (41*a*). In uniaxial strain the yield condition can be incorporated in $F(S_i, \overline{p})$ in eq. (76). For this geometry eq. (76) can be replaced by a single equation:

$$\mathrm{d}p_x/\mathrm{d}t = a^2(\mathrm{d}\varrho/\mathrm{d}t) - F(p_x, \varrho)\,, \tag{77}$$

where a is the elastic sound speed at density ϱ.

In Sect. 2 we combined the flow equations, eqs. (1)-(3), under the assumption $p = p(\varrho)$, to form a set of characteristic equations, eqs. (25) and (26). A similar procedure can be executed in the present case. Combining eqs. (1), (2) and (77) yields the characteristic set:

$$C+: \quad \mathrm{d}p_x + \varrho a\,\mathrm{d}u = -F\,\mathrm{d}t\,, \qquad \mathrm{d}x/\mathrm{d}t = u + a\,, \tag{78}$$

$$C-: \quad \mathrm{d}p_x - \varrho a\,\mathrm{d}u = -F\,\mathrm{d}t\,, \qquad \mathrm{d}x/\mathrm{d}t = u - a\,, \tag{79}$$

along with eq. (77), which applies along the particle path, sometimes called the « C_0 characteristic »:

$$\mathrm{d}p_x - a^2\,\mathrm{d}\varrho = -F\,\mathrm{d}t\,, \qquad \mathrm{d}x/\mathrm{d}t = u\,. \tag{80}$$

The characteristic equations are less useful for this and other time-dependent constitutive relations than for time-independent relations because there are now no quantities which remain constant on characteristics. This means that wave transitions are no longer limited to specific curves in the (p, u) plane, as described in Sect. 3, and that type of analysis loses most of its utility. The characteristic equations can still be used in numerical analysis, though it is almost always simpler to use a von Nuemann-Richtmyer procedure.

The principal observable effect of eq. (77) on the shock wave is decay of the elastic precursor. The nature of this decay can be seen by an approximate analysis. Suppose the precursor is never of such large amplitude that its speed of propagation differs significantly from the ambient elastic speed a_0. Then the jump condition for the precursor becomes (eq. (5)):

$$p_x = \varrho_0 a_0 u$$

and when the precursor amplitude decays by $\mathrm{d}p_x$, the particle velocity behind

the precursor decays by an amount

$$du = dp_x/\varrho_0 a_0 . \tag{81}$$

Under the assumed conditions, eq. (78) also applies along the path of the precursor. Combining eqs. (78) and (81) yields the relation

$$dp_x/dt = -F/2 . \tag{82}$$

The function F is expected in general to be quite complicated. We can get a qualitative picture of its effect by assuming the form, for compression only,

$$F = (p_x^e - p_x^s)/T , \qquad p_x^e > p_x^s, \tag{83}$$

where $T =$ constant. Compression by the precursor is assumed to be elastic, so p_x of eq. (82) lies on a metastable extension of the elastic compression curve, $p_x^e(V)$. Above the yield point there is a stress $p_x^s(V)$ which will finally be reached for the given volume V after a very long time. This is curve AB of Fig. 14 *b*). According to eqs. (82) and (83), decay of the precursor amplitude, $p_x \equiv p_x^e(V)$ continues until $p_x^e(V) = p_x^s(V)$, which occurs at the static value of the Hugoniot elastic limit. To see the effect more explicitly, note that

$$(d/dt)(p_x^e - p_x^s) = (1 - c^2/a^2)(dp_x^e/dt) , \tag{84}$$

where $c^2 = K/\varrho$, $a^2 = (K + 2\mu/3)/\varrho$. If Poisson's ratio, ν, is independent of density, so is c^2/a^2. Then eqs. (82)-(84) can be integrated to yield

$$p_x^e(V) - p_x^s(V) = (p_x^e - p_x^s)_0 \exp[-x/x_0] , \tag{85}$$

where

$$x_0 = 2TD/(1 - c^2/a^2) . \tag{86}$$

Integrating eq. (84) under the assumption that $\nu =$ constant enables us to simplify eq. (85):

$$p_x^e - p_{\mathrm{HEL}}^s = (p_x^e - p_{\mathrm{HEL}}^s)_0 \exp[-x/x_0] , \tag{87}$$

where p_{HEL}^s is the static value of the Hugoniot elastic limit, related to the static yield strength by eq. (47).

Equation (82) was derived on the assumptions that the precursor follows a characteristic and that the energy equation, eq. (3), does not affect the prop-

agation process. A more rigorous expression can be obtained by combining eq. (77) with eqs. (1)-(3) and specializing the result along the shock path [8]:

$$\frac{\mathrm{D}p_x}{\mathrm{D}x} = \left(1-\frac{u}{D}\right)\frac{(D-u)^2-a^2}{\frac{3}{2}(D-u)^2+a^2/2}\frac{\partial p_x}{\partial \mathrm{x}} - \frac{(D-u)^2}{D}\frac{F'}{\frac{3}{2}(D-u)^2+a^2/2}, \tag{88}$$

$$F' = (1-\alpha\Gamma y/2\mu)F\,. \tag{89}$$

Here the block derivative, $\mathrm{D}/\mathrm{D}x$, refers to differentiation along the shock path, $\partial p_x/\partial x$ is evaluated immediately behind the precursor front, and F' is a modification to F resulting from the assumption that a fraction α of plastic work goes into heat. In eq. (89), Γ is the Gruneisen parameter. F' and F differ by less than 10 % for metals in which plastic flow occurs.

Under the assumptions that $D-u=a$ and $\alpha=0$, eq. (88) reduces to eq. (82).

Considerable effort in recent years has been devoted to attempts to relate the relaxation function F of eq. (75) to the motion and multiplication of dislocations. The basic relation is

$$\mathrm{d}E^p/\mathrm{d}t = hNbv = F/2\mu\,, \tag{90}$$

where N is the number of dislocations per unit area, b is the Burgers vector, h is a numerical constant the order of units, and v is the mean velocity of dislocations. Since $E_p = 2\varepsilon_1/3$ in uniaxial strain, eq. (90) becomes

$$\mathrm{d}\varepsilon_1/\mathrm{d}t = 3hNbv/2\,. \tag{91}$$

There are various models for multiplication and motion of dislocations. One which is frequently used is due to GILMAN:

$$N = N_{om}(1+A\varepsilon^p)\,, \tag{92}$$

$$v = v_{\max}\exp\left[-D/\tau\right], \tag{93}$$

where

N_{om} = initial density of mobile dislocations,

$v_{\max}$ = maximum dislocation velocity $\sim v_{\mathrm{shear}}$,

D = drag coefficient,

A = multiplication coefficient,

τ = resolved shear stress $= (p_x-p_y)/2$.

To the extent that eq. (82) applies, no multiplication occurs in the front of the elastic precursor, so the value of A is of no consequence in determining the precursor decay. A set of decay curves for single crystal tungsten are shown

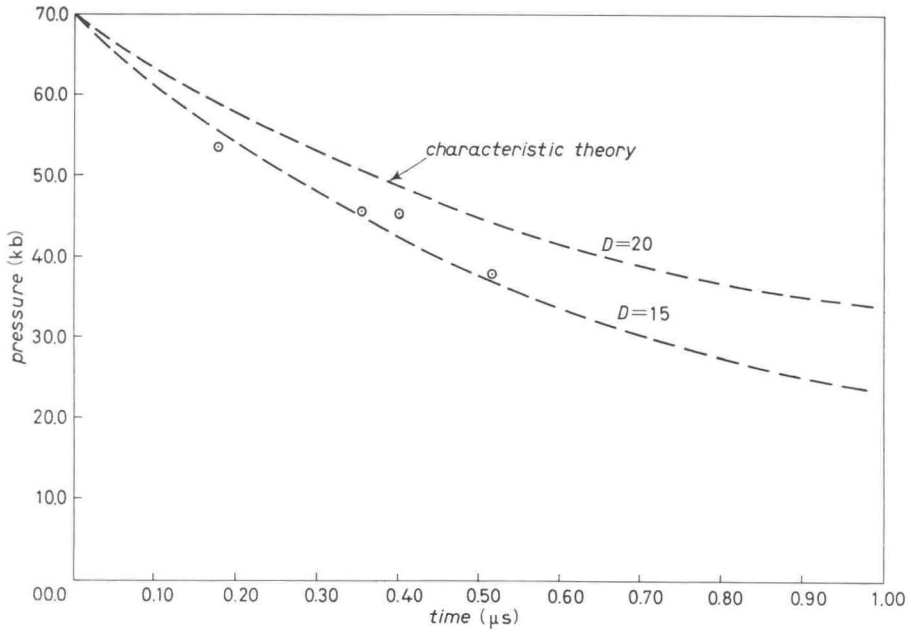

Fig. 20. – Precursor decay in single crystal tungsten, courtesy of T. E. MICHAELS, W.S.U. (unpublished).

in Fig. 20 for different values of the drag coefficient D. Here, as in work reported elsewhere, it is necessary to assume a value of N_{om} much higher than the measured values in order to get reasonable agreement with experiments.

In order to see the effect of dislocation multiplication, one must record the wave profile between the elastic precursor and the plastic shock. Such a profile obtained with a quartz gauge on LiF is shown in Fig. 21. By adjusting the parameter A in eq. (92), the sharp drop in amplitude immediately following the elastic peak can be explained.

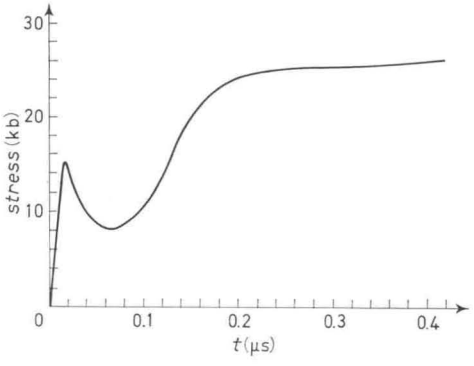

Fig. 21. – Precursor and shock in LiF. (J. ASAY, W.S.U.).

It is not yet clear whether critical tests of dislocation theory can be made from shock profile meas-

urements. There is not yet any clear-cut evidence that dislocations bear any relation to elastic-plastic behavior in shock. It appears, however, that the subject is worth pursuing in depth for at least one case until a definitive answer appears.

7. – Irreversible phase transitions.

Equilibrium phase transitions were discussed in Sect. **5** and a formal procedure for integrating the flow equations through the mixed-phase region was described. The central relations are given in eqs. (61) and (62) together with the equilibrium assumption, eq. (64). When considering the irreversible case we need to re-examine the assumptions made in obtaining eqs. (61) and (62). In a general sense it is possible to have irreversible mass transfer, irreversible heat transfer and irreversible work transfer between the two phases. The first of these occurs if the reaction parameter f is out of equilibrium, the second if temperatures of the two phases are unequal and adiabaticity is violated, the third if pressures in the two phases are out of equilibrium. Of these three it is quite easy to imagine f out of equilibrium; this is in fact probably the usual case since the deviation of f from equilibrium corresponds to a value of the Gibbs energy above the minimum and this acts as a force to drive the reaction toward equilibrium.

If nucleation of the second phase occurs at very many points in every volume element so that dimensions of crystals in either phase are very small, it is unlikely that pressure will be significantly out of equilibrium. Temperature equilibration, however, takes place relatively slowly and in any particular case it may well call for a closer examination. However as an approximation at this stage it looks reasonably good and preferable to the other simple alternative that no heat exchange whatsoever occurs between phases. Equations (54) and (55) represent another possible source of error inasmuch as the interfacial energy between phases is ignored. Here again it seems unlikely that the effect will be large, and it seems appropriate to ignore it for the present. With assumptions unchanged from those previously made, we again arrive at eqs. (61) and (62) with coefficients the same as before. It's important to note that both here and in Sect. **5** it is assumed that both phases have the same particle velocity, u. This is appropriate for solid-solid transitions; it would not be appropriate for gas-liquid or gas-solid transitions.

The difference between the treatment of reversible and irreversible transitions then reduces to the computation of f. In Sect. **5** f was computed from the Clausius-Clapeyron equation (eqs. (64) and (65)). In the irreversible case we assume that

$$\mathrm{d}f = g(V, T, f)\,\mathrm{d}t\,. \tag{93}$$

Equations (61), (62) and (93) form the constitutive relations for the irreversible transition when $0 < f < 1$. If $f = 0$ or 1, eqs. (56) apply. This formulation of the transition process is particularly appropriate for the von Neumann-Richtmyer integration since in that procedure dt is specified explicitly.

The above formulation represents the following physical model. Each phase has an equation of state surface in (p, V, T) space, and in equilibrium the surfaces are separated by the mixed phase region; V, for example, is never double-valued. We now suppose that each phase is defined for all p and T and that V may lie on either surface, one of which is metastable, or may take any value between the two surfaces. The value it has at any moment is determined by its previous value, by dt, by the equation of continuity, and by previous values of p, T and f; and it seeks an equilibrium state through the operation of eq. (93) until it arrives at an equilibrium surface where $f = 1$ or 0.

As an example of the application of these equations, consider the case of iron, which has a transition from *bcc* to *hcp* at 130 kb and approximately room temperature. For the transition we assume that:

$$V_2(p, T) - V_1(p, T) = -0.0059 \text{ cm}^3/\text{g} \tag{94a}$$

$$\text{static transition pressure, } p_t = 130 \text{ kb}, \tag{94b}$$

$$dp_t/dT = -0.065 \text{ kb}/^\circ\text{K}, \tag{94c}$$

$$df/dt = (f_{eq} - f)/\tau, \tag{94d}$$

$$f_{eq} = (V - V_1)/(V_2 - V_1) \text{ at } p \text{ and } T, \tag{94e}$$

$$\tau = \tfrac{1}{3} \mu\text{s}. \tag{94f}$$

A constant pressure of 200 kb is applied to the surface of a half-space at $t = 0$ and we seek the wave profile at subsequent times and the rate of decay of the precursor wave associated with the transition. The elastic precursor is ignored.

The integration was performed by a modification of the von Neumann-Richtmyer method [9]. The development of the pressure profile at early times is shown in Fig. 22 and the fully developed double wave is shown in Fig. 23. In each figure the effect of changing $V_2 - V_1$ is shown; it influences the shape of the profile but not the decay rate. The decay of the elastic precursor is shown in Fig. 24. The computation was also made with $dp_t/dT = 0$ with no substantial change in the results. The dashed line shown in Fig. 24 fits the decay curve obtained by numerical integration reasonably well. It was obtained analytically in the following way:

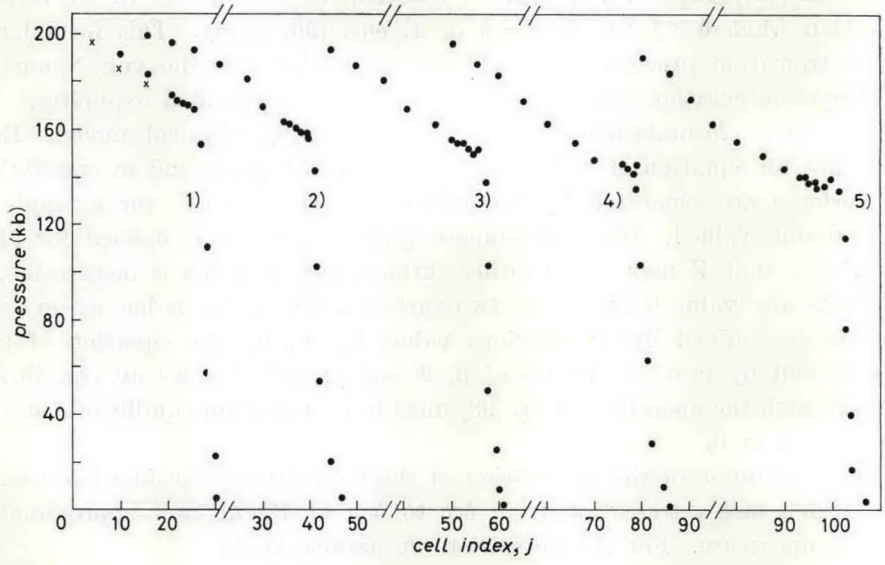

Fig. 22. – Pressure profiles at early times. (Ref. [9]). $p_1 = 0.200$ Mb; cell width = $= 0.01$ cm; $\tau = \frac{1}{3}$ μs; 1) $t = 0.526$ μs; 2) $t = 0.812$ μs; 3) $t = 1.105$ μs; 4) $t = 1.554$ μs; • $\Delta V = -0.004$ cm³/g; × $\Delta V = -0.0059$ cm³/g.

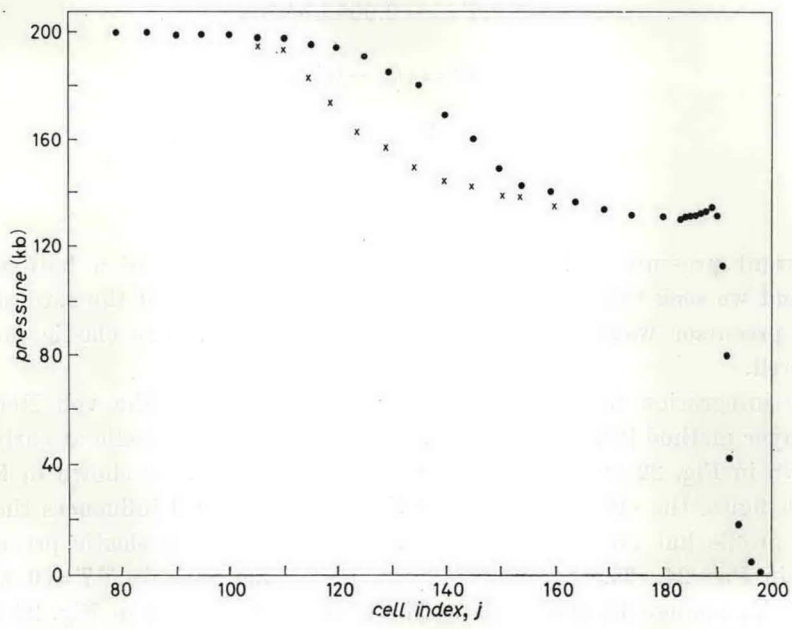

Fig. 23. – Double shock in iron. (Ref. [9]). $p_1 = 0.200$ Mb; cell width = 0.01 cm; • $\Delta V = -0.004$ cm³/g; × $\Delta V = -0.0059$ cm³/g; $\tau = \frac{1}{3}$ μs.

Assume the entire process to be temperature independent. Then eqs. (61) and (94*d*) can be combined in the form

$$(95) \qquad \mathrm{d}p/\mathrm{d}t = a^2\,\mathrm{d}\varrho/\mathrm{d}t + [(m_1 n_2 - m_2 n_1)/(l_1 m_2 - l_2 m_1)](f_{eq} - f)/\tau\,,$$

where m_1, n_1, etc., are as defined in Sect. **5** and a is the frozen sound speed, *i.e.*, $\sqrt{\mathrm{d}p/\mathrm{d}\varrho}$ with $f =$ constant. Equation (95) is then identical in form to the stress-relaxation equation, eq. (77). Following the procedure described there, we form the characteristic equations, assume the first shock velocity is equal to sound speed, and obtain

$$(96) \qquad \mathrm{d}p_1/\mathrm{d}t = -[(m_1 n_2 - m_2 n_1)/(l_1 m_2 - l_2 m_1)]\cdot(f_{eq} - f)/2\tau\,,$$

where p_1 is the amplitude of the transition shock. Assuming $\Delta V = V_2 - V_1 =$ = constant as before and $C_{p1} = C_{p2}$, eq. (96) becomes

$$(97) \qquad \mathrm{d}p_1/\mathrm{d}t = -(\Delta V f_{eq}/2\tau)\,\mathrm{d}p_1/\mathrm{d}V.$$

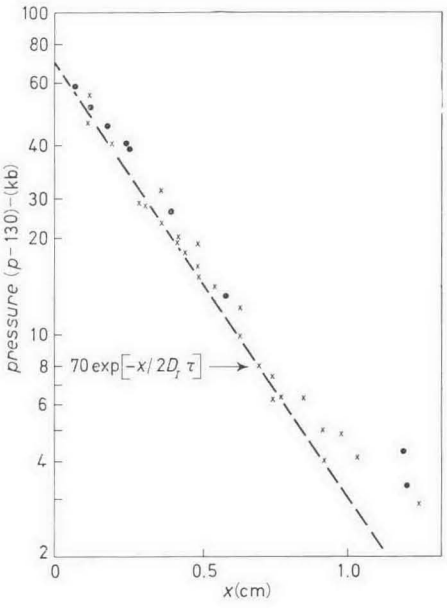

Fig. 24. – Decay of α-phase wave in iron. (Ref. [9]). Driving pressure = 200 kb; $\tau = \frac{1}{3}$ μs; $D_I\tau = 0.17$ cm; • temperature-independent; × temperature-dependent.

Here we have assumed that $f = 0$, *i.e.*, the material is in the metastable first phase at the peak of the first shock. If $\mathrm{d}p_1/\mathrm{d}V =$ constant, eq. (94*e*) gives

$$(98) \qquad f_{eq} = \begin{cases} 1\,, & V_1 \leqslant V_t) + \Delta V, \\ (V_1 - V_t)/\Delta V = [(p_1 - p_t)/\Delta V]\,\mathrm{d}V_1/\mathrm{d}p\,, & V_t + \Delta V \leqslant V_1 \leqslant V_t, \\ 0\,, & V_t \leqslant V_1, \end{cases}$$

where V_t, p_t represent the intersection of the phase 1 Hugoniot with the mixed-phase boundary. Combining eqs. (97) and (98) and integrating gives

$$(99a) \qquad p_1 = p_0 - (x\Delta V/2D_1\tau)\,\mathrm{d}p_1/\mathrm{d}v\,, \qquad V_1 \leqslant V_t + \Delta V,$$

$$(99b) \qquad = p_t + (p_0 - p_t)\exp[-x/2D_1\tau]\,, \qquad V_t + \Delta V \leqslant V_1 \leqslant V_t,$$

$$(99c) \qquad = p_t\,, \qquad V_1 = V_t,$$

where $x = D_1 t$, D_1 is the first shock velocity, and p_0 is the driving pressure. For $p_0 = 200$ kb, eq. (99*b*) applies. The result is shown in Fig. 24.

The graphs in Fig. 22-24 were calculated with $\tau = \frac{1}{3}\,\mu$s. In order to determine the relation between rise time in the second shock and τ, the constitutive relations can be combined with eqs. (4)-(6) to determine the steady profile in the second shock. The result of that integration is that the rise time $= 2.25\tau$. Unfortunately the theory of the rates at which solid-solid phase transitions occur is not developed to the state where predictions of experimental results can be made or where experimental results can be used to determine physical parameters. It is evident that careful experiments and creative theoretical work are both required in this area.

8. – Mechanical effects.

The most obvious terminal effects of shock experiments in solids are fractures produced by wave interactions. The geometry of fracture depends principally on the paths of intersecting tensile waves; limiting conditions for fracture are determined by dynamic strength of the material, which may depend on geometry and certainly depends upon stress rate or strain rate.

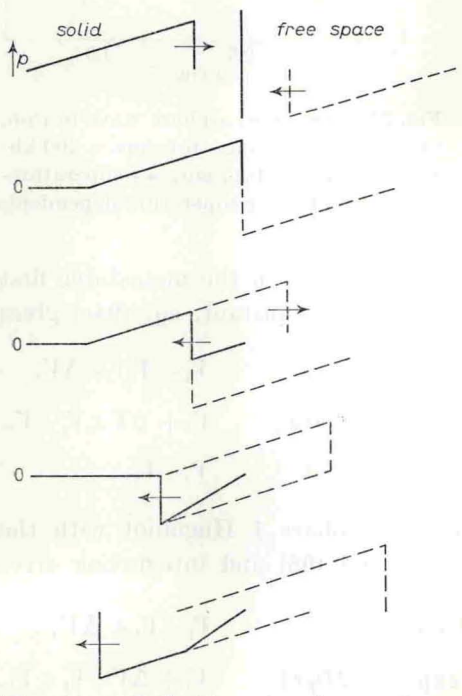

Fig. 25. – Reflection at a free surface, linear waves.

The geometry is indicated in Fig. 25 and 26 for the simplest case, plane spall. In Fig. 25 are shown a sequence of pressure profiles of a compressive pulse approaching and being reflected from a free surface. Propagation and interactions are assumed linear for purposes of illustration. The solid curve is the real pressure profile; the dashed curves represent the pulses from which it is composed. The interaction of the rarefaction in the incident pulse with the reflected rarefaction from the free surface produces tensile stresses in the specimen. If these produce the conditions required for fracture at any point and time, fracture is initiated at that point and time. This is illustrated more precisely in Fig. 26. In 26 *a*) is shown an (x, t) diagram for the process of Fig. 25. The incident shock, $\mathscr{S}_+$, is

followed by a simple wave rarefaction represented by the fields 11, 12, 13, separated by C_+ characteristics. The free surface, ABC, is immediately accelerated at the incidence of $\mathscr{S}_+$ and a back-ward-facing rarefaction fan, $\mathscr{R}_-$, centered at B, is generated. The C_+ characteristics pass through the fan of the reflected rarefaction and each in turn is reflected from the free surface as shown. The map of the flow in the (p, u) plane is shown in Fig. 26 *b*).

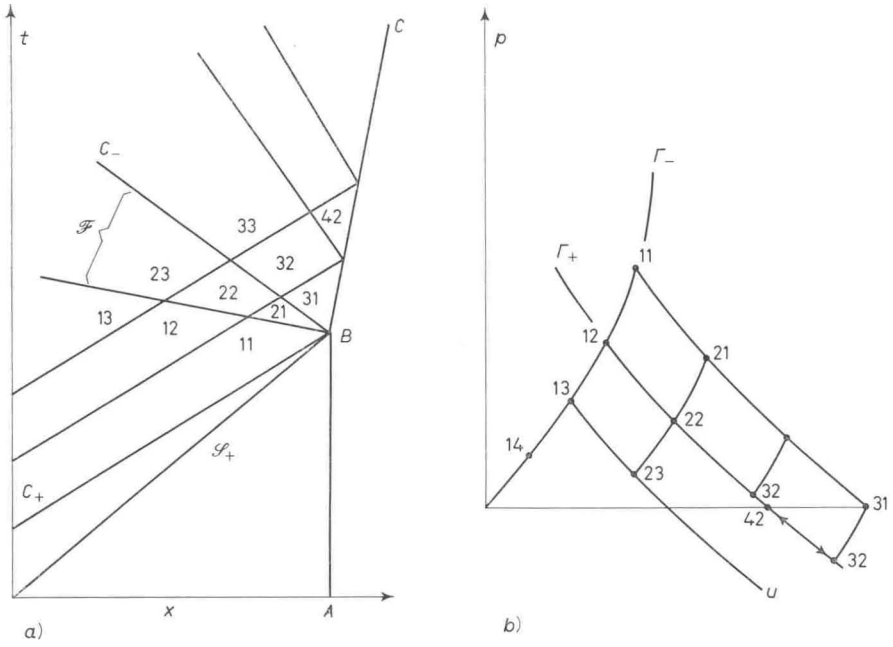

Fig. 26. – Reflection at a free surface. *a*) (x, t) plane; *b*) (p, u) plane.

The point to note here is that the transition from the field 12 to the free surface state takes place along a Γ_+ characteristic, and that the mapping goes into the negative pressure region and returns to the $p = 0$ state at 42. This is in qualitative agreement with the sketches of Fig. 25.

Whether or not a spall occurs depends upon the magnitude and duration of the stress. BREED, MADER and VENABLE have found [10] that spall occurs if the fracture stress, σ_f, satisfies the relation

$$\sigma_f = A + F(\Delta\sigma/z)^{\frac{1}{2}}, \tag{100}$$

where z is the distance from the free surface at which spall occurs, $\Delta\sigma = \sigma_f$, and $\Delta\sigma/z$ is the stress gradient. A and B are material constants. Equation (100) implies that fracture occurs when $\sigma\Delta t$ reaches a characteristic value.

BUTCHER, BARKER, MUNSON and LUNDERGAN have proposed a slightly more general relation which includes the above [11]; fracture occurs when

$$\Delta t \sigma^r = G \,, \tag{101}$$

where r and G depend on the material.

A still more general relation has been used by F. TULER [12] to describe experiments in 6061T6 Al; fracture occurs at time t_f defined by the relation

$$\int_0^{t_f} (\sigma_0 - \sigma)^r \, \mathrm{d}t = G \,, \tag{102}$$

where $r = 2.02$, $G = 3.98 \cdot 10^{13}$, $\sigma_0 = -10^{10}$ dyn/cm^2. All of these rules apply to plane spall, described in Fig. 25 and 26. None have any particularly sound theoretical basis. Present efforts in this area are directed toward experiments which will provide information for nucleation and growth models similar to those discussed by MCCLINTOCK [13].

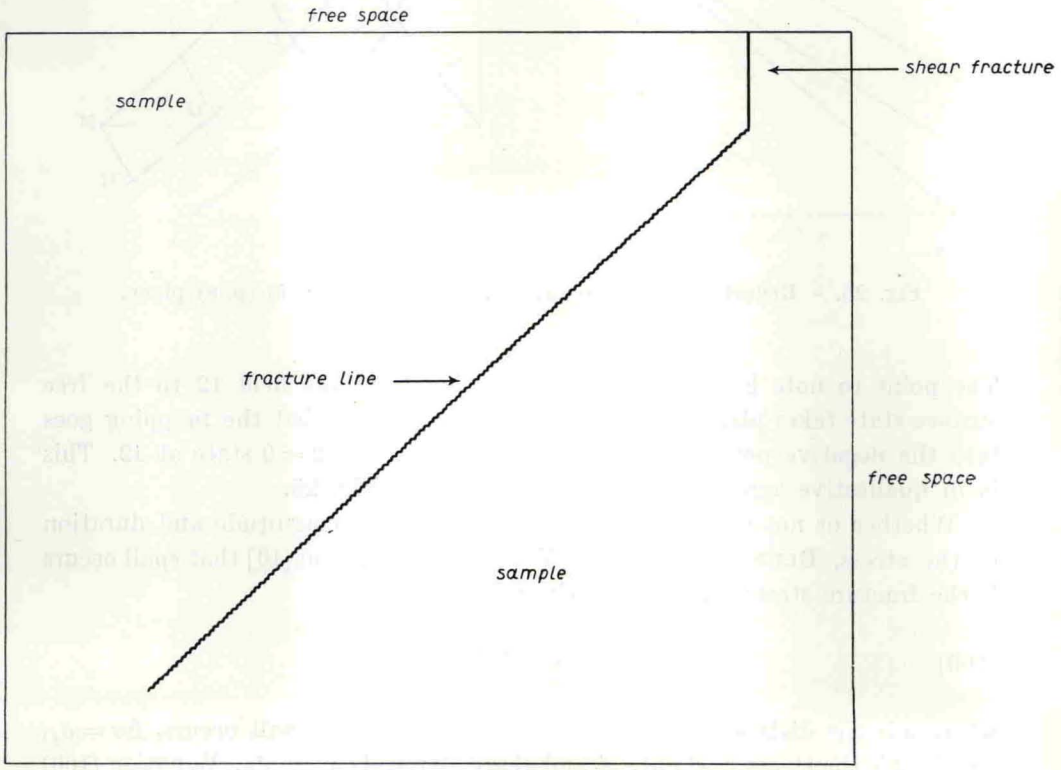

Fig. 27. – Ridge cut.

Another common phenomenon is the « ridge fracture »: any corner in a shocked sample may be neatly split, except near the outermost tip, where common shear fracture normally occurs, Fig. 27. These have been discussed in detail by RINEHART and PEARSON [14] and by FOWLES and ANDERSON [15]. The latter have performed a linear elastic analysis of the configuration shown in Fig. 28 and 29. In Fig. 28 the line labelled Φ represents a compressive wave

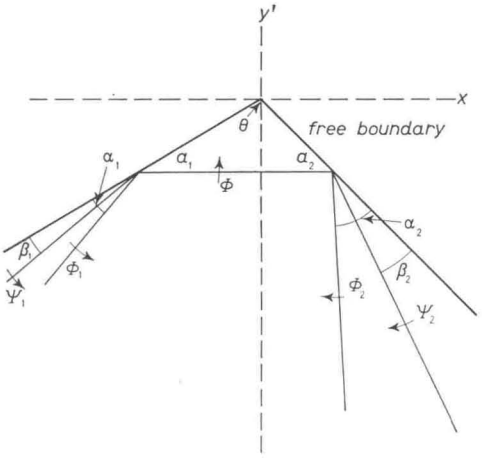

Fig. 28. – Wave incident upon corner. (From ref. [15]).

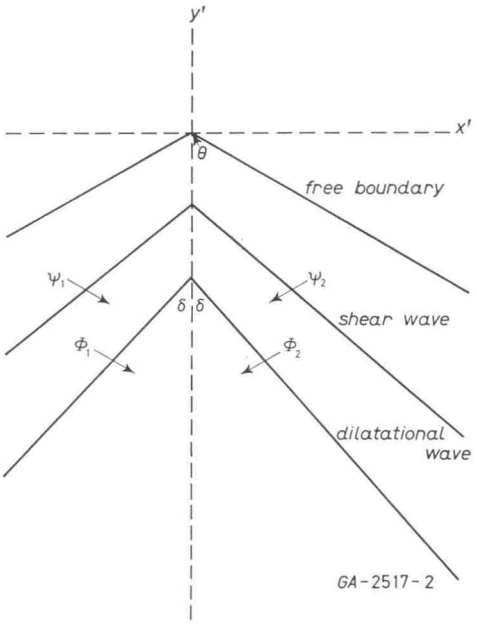

Fig. 29. – Interaction of reflected waves. (From ref. [15]).

running into a corner, generating reflected dilatation and shear waves Φ_1, Φ_2, and ψ_1, ψ_2, respectively. At a later time, shown in Fig. 29, only the reflected waves remain, and these meet along the dotted axis labelled y', the points of intersection running down as time progresses. The interacting tensile waves, Φ_1 and Φ_2 and/or shear waves ψ_1 and ψ_2 produce a fracture running along y' if the amplitude of the incident wave is sufficiently great. Their analysis, which agreed reasonably well with experiments, indicated that, for a given incident wave, the maximum fracture stresses were developed for $\theta \simeq 120°$. The shear fracture near the corner in Fig. 27 is very likely due to the finite time required for fracture, as in eqs. (100)-(102).

An interesting type of fracture occurs when a layer of explosive is detonated in contact with a metal plate. The situation is characterized in Fig. 30. In Fig. 30 *a*) the detonation front is travelling with speed D across the surface

of the plate, inducing a trailing shock, $\mathscr{S}$. Pressure on the plate falls quickly behind the detonation front as indicated. This produces a corresponding rarefaction behind $\mathscr{S}$. The shock $\mathscr{S}$ is reflected from the bottom surface as a rarefaction, $\mathscr{R}$, and the interaction of $\mathscr{R}$ with the rarefaction behind $\mathscr{S}$ produces a tension stress field which may be strong enough to fracture the plate along

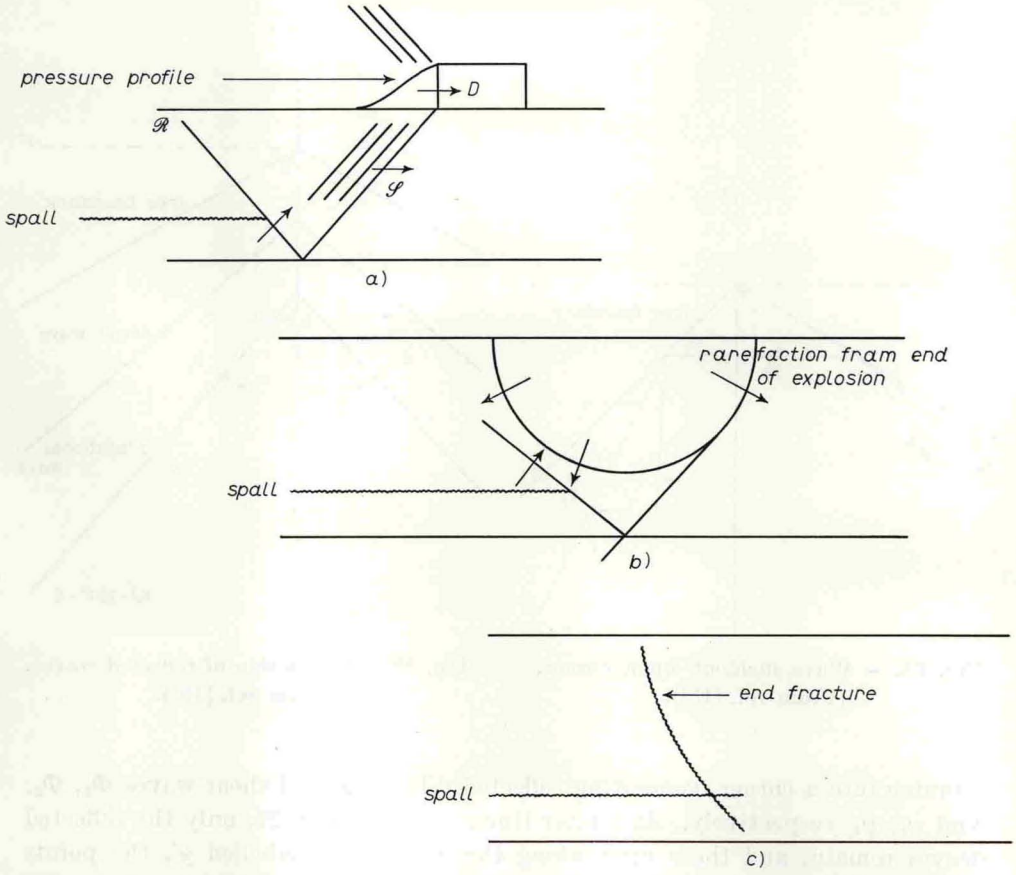

Fig. 30. – Generation of end fracture. *a*) Steady waves from detonating explosive; *b*) rarefaction generated at end of explosive intersects with bottom rarefaction; *c*) end fracture resulting from interaction.

the surface labelled « spall ». When the detonation reaches the end of the explosive charge, a rarefaction is generated with a more or less circular wave front as shown in Fig. 30 *b*). This rarefaction, interacting with $\mathscr{R}$, produces a stress field which results in an end fracture with orientation shown in Fig. 30 *c*). The geometry of this interaction has been worked out [16], but no one has

yet calculated the stress fields and correlated them with experiments or with fracture formulae.

An interesting property of iron and carbon steels is their propensity to fracture under explosive or projectile impact so as to produce a very smooth surface. This fracture is called the « smooth spall » and has been described by RINEHART and PEARSON [14], by ERKMAN [17], by LETHABY and SKIDMORE [18], and by TUPPER [19]. In the last three works the smooth spall is attributed to the interaction of rarefaction shocks associated with the α-ε phase transition in iron.

9. – Shock waves on a one-dimensional lattice of mass points.

The mass points are connected by nonlinear springs, as in Fig. 31, and by dashpots. The forces exerted by the former on the N-th point mass are denoted

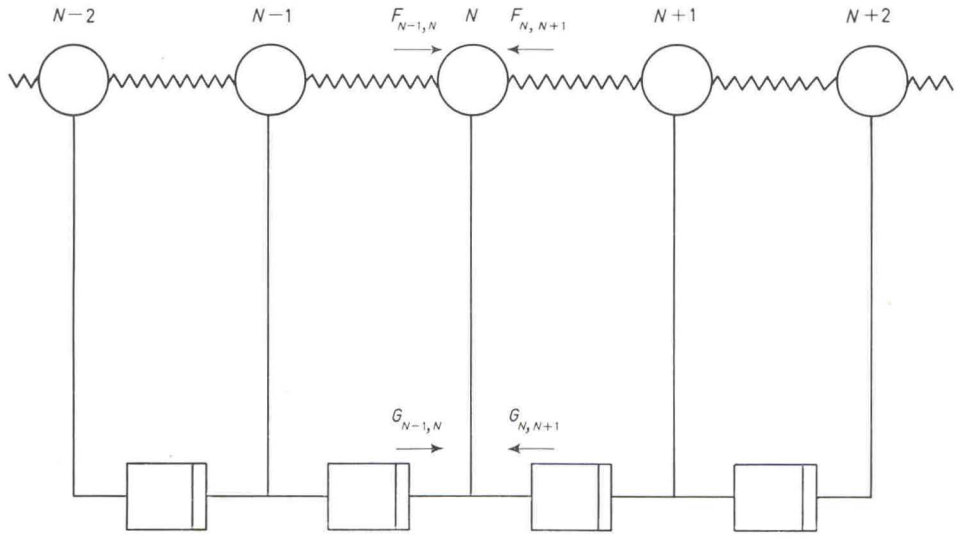

Fig. 31. – Dissipating lattice model. $\mathrm{d}^2X_N/\mathrm{d}T^2 = F_{N-1,N} - F_{N,N+1} + G_{N-1,N} - G_{N,N+1}$.

by $F_{N-1,N}$ and $F_{N,N+1}$; those associated with the dashpots are $G_{N-1,N}$ and $G_{N,N+1}$. The equation of motion of the N-th particle is

$$\mathrm{d}^2X_N/\mathrm{d}T^2 = F_{N-1,N} - F_{N,N+1} + G_{N-1,N} - G_{N,N+1}\,, \tag{103}$$

where X_N is its position at time T; X and T are reduced values corresponding to unit mass and unit equilibrium separation between mass points. The lattice

is supposed to extend from $N=1$ to ∞ and we imagine the first mass point to be given a velocity u_1 at $T=0$. The entire lattice is assumed quiescent before that. For a parabolic force law,

$$(104)\quad F_{N,N+1} = -(S_{N+1} - S_N) + \alpha(S_{N+1} - S_N)^2, \qquad S_N = X_N - 1, \qquad G_{N,N+1} = 0,$$

the acceleration of the N-th particle is shown in Fig. 32 [20]. The broken line shown there is the result of a numerical integration, the dashed line is

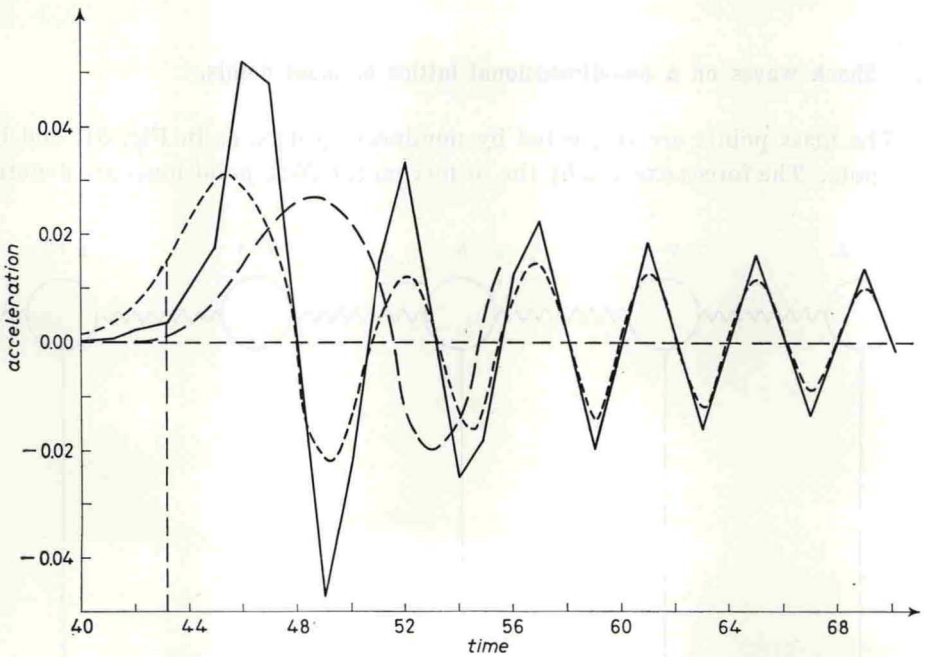

Fig. 32. – Acceleration of a mass point in a nonlinear lattice. (Ref. [20]).

an analytic approximation obtained by averaging the nonlinear force term over time, and the long-dashed line is the exact solution when the coefficient $\alpha=0$ in eq. (104). If solutions are compared for successively larger values of N, it is found that the initial acceleration increases monotonically with N and that the rate of decay of the oscillation decreases monotonically. This suggests that the solution may be approaching a permanent regime:

$$(105)\qquad S_N(T) = S(T - N\theta),$$

where θ is a constant equal to the reciprocal wave speed. When eq. (105) is

substituted into (103) with the force law of (104), we obtain

$$(106)\quad d^2S/dy^2 = [S(y-\theta) - 2S(y) + S(y+\theta)]\cdot\{1-\alpha[S(y-\theta) - S(y+\theta)]\},$$

where

$$y = T - N\theta .$$

Equation (106) is an uncommon type of differential-difference equation and is not readily solved, even numerically. An approximate solution can be found by expanding $S(y\pm\theta)$ in powers of θ and retaining fourth order terms. If dissipation is nonzero, however small, nearly-steady oscillations of the type suggested by Fig. 32 are obtained. The frequencies of oscillation predicted by the approximate theory are, however, quite different from those obtained from numerical integration of the transient equations. It thus appears that this picture of the permanent regime in the lattice is qualitatively correct, but that eq. (106) must be solved if parameters of the permanent regime are to be calculated [21].

One interesting application of these results is to the von Neumann-Richtmyer integration of the flow equations. If artificial viscosity is too small, the results of such an integration oscillate wildly. This has sometimes been interpreted as instability of the numerical integration procedure; it is in fact the true physical behavior of the lumped-constant system used to model the continuum for purposes of numerical integration.

REFERENCES

[1] R. Courant and K. O. Friedrichs: *Supersonic Flow and Shock Waves* (New York, 1948). This contains much material basic to Sects. **1-3.**

[2] G. E. Duvall: *Les ondes de détonation* (Paris, 1962), p. 337.

[3] D. R. Bland: *Journ. Inst. Math. Appl.*, **1**, 56 (1965).

[4] J. O. Erkman and G. E. Duvall: *Developments in Mechanics*, edited by T. C. Huang and M. W. Johnson Jr., vol. **3**, Pt. 2 (New York, 1965), p. 179.

[5] W. Herrmann: *Wave Propagation in Solids* (New York, 129), p. 129.

[6] G. E. Duvall and Y. Horie: *Proc. Fourth Symposium on Detonation, Oct. 12-15, 1965* (Washington, D. C., 1966), p. 248.

[7] R. D. Richtmyer and K. W. Morton: *Difference Methods for Initial-Value Problems*, 2nd Ed. (New York, 1967).

[8] T. J. Ahrens and G. E. Duvall: *Journ. Geophys. Res.*, **71**, No. 18, 4349 (1966).

[9] Y. Horie and G. E. Duvall: *Proc. Army Symposium on Solid Mechanics, 1968*, p. 127; available from Applied Mechanics and Research Laboratory, Army Materials and Mechanics Research Center, Watertown, Mass.

[10] B. R. Breed, C. L. Mader and D. Venable: *Journ. Appl. Phys.*, **38**, 3271 (1967).
[11] B. M. Butcher, L. M. Barker, D. E. Munson and C. D. Lundergan: *Am. Inst. Aeronautics and Astronautics Journ.*, **2**, 977 (1964).
[12] F. W. Tuler: Sandia Laboratories, Albuquerque, N. Mex., private communication.
[13] F. A. McClintock: *International Journ. Fract. Mech.*, **4**, 101 (1968).
[14] J. S. Rinehart and J. Pearson: *Behavior of Metals Under Impulsive Loads* (New York, 1954).
[15] G. R. Fowles and G. D. Anderson: Poulter Laboratories Internal Report 032-59, Stanford Research Institute, Menlo Park, Calif. (1959).
[16] W. E. Drummond: *Comments on the cutting of metal plates with high explosive charges*, paper no. 57-A-89, American Society of Mechanical Engineers, 345 E. 47th St., New York, N. Y. 10017 (1957).
[17] J. O. Erkman: *Journ. Appl. Phys.*, **32**, 939 (1961).
[18] J. Lethaby and I. C. Skidmore: S.W.A. Branch Note No. 3/59, AWRE, Aldermaston, Berks. (March 1959).
[19] S. J. Tupper: *On the propagation of plane stress waves generated in a thick steel plate by a surface explosion*, A.R.D.E. Report (B) 12/61 (Sept. 1961).
[20] R. Manvi, G. E. Duvall and S. C. Lowell: *Int. Journ. Mech. Sci.*, **11**, 1 (1969).
[21] G. E. Duvall, R. Manvi and S. C. Lowell: *Journ. Appl. Phys.*, **40**, 3771 (1969).